

Original Study

Open Access

Mohanad Talal Alfach*

Seismic Structure-Soil-Structure Interaction (SSSI) between piled neighboring bridges: Influence of height ratio

<https://doi.org/10.2478/sgem-2024-0003>

received January 15, 2023; accepted February 17, 2024.

Abstract: This paper explores the impact of height ratios on the seismic Structure-Soil-Structure Interaction (SSSI) for three adjacent bridges with varying superstructure masses ($M_{st} = 350, 1050, 350$ t) through 3D numerical simulations. A comprehensive series of numerical analyses has been conducted across different height ratios ($R = 1, 1.1, 1.15, 1.2, 1.25, 1.5, 2, \text{ and } 3$) to assess their influence on superstructure acceleration and the internal forces within the foundation piles. The bridges under investigation are supported by groups of piles embedded in nonlinear clay. The numerical simulations were executed using fast Lagrangian analysis of continua in three dimensions (FLAC 3D), a three-dimensional finite differences modeling software. The findings revealed that variations in mass ratios significantly impact the SSSI effects on superstructure acceleration and pile internal forces. Notably, adverse effects were more pronounced for mass ratios of $R = 1.1$ and 1.2 , leading to an increase in bending moment, shear force, and superstructure acceleration by up to 237.8%, 291.4%, and 70.33%, respectively. In contrast, a mass ratio of $R = 3$ resulted in a decrease in bending moment, shear force, and superstructure acceleration by up to 72%, 82.14%, and 81.13%, respectively. This implies that a careful arrangement of adjacent structures with different masses can be employed effectively to manage the (SSSI) effects.

Keywords: SSSI; different superstructure masses; height ratios; dissimilar adjacent bridges; nonlinear; seismic; three dimensional.

1 Introduction

As most structures in densely populated urban areas are constructed in clusters, and often with only a few meters apart, their seismic response is thoroughly affected by the dynamic behavior of the adjacent structures and their fundamental dynamic characteristics; this interaction is termed as Structure-Soil-Structure Interaction (SSSI). Whence, the study of the (SSSI) effects has become increasingly inevitable to ensure an effective earthquake resilience of the structures constructed in dense urban environments. Furthermore, the accelerated lack of available space has led in some cases to construct new large structures near old smaller structures in new neighborhoods, which impose additional complications to the (SSSI) effects. The state of the art in (SSSI) analysis has been mostly concentrated on tall buildings and skyscrapers; the effect between neighboring bridges has been rarely studied, mainly due to the shortage of experimental or field-based case studies that confirm its effect on seismic response. The numerical analyses presented herein share the common goal of a better understanding of the phenomena of (SSSI), with particular attention to focusing on the effect of (SSSI) between three dissimilar adjacent bridges, different superstructure mass ratios, inter-bridge spacing, and the arrangement of the bridge toward the seismic loading direction.

SSSI has attracted extensive attention in the last decades; most previous research about (SSSI) has generally concentrated on the seismic behavior of neighboring tall buildings and skyscrapers. Nevertheless, there is rather a variance between the findings of these studies in the literature. In the numerical field, Kim [1] has employed a three-dimensional (3D) finite element (FE) model to analyze the seismic interaction between three connectors and the surrounding soil at different bridge superstructure elevations of an existing bridge interchange at the intersection of interstates 10 and 215 (San Bernardino, CA, USA). Bolisetti and Whittaker [2] performed a series of numerical simulations and centrifuge

*Corresponding author: Mohanad Talal Alfach, School of Mathematics, Computer Science and Engineering, Department of Civil Engineering City, University of London, UK, E-mail: mohanad.alfach@yahoo.com

experiments to assess the seismic effects of (SSSI) on buildings constructed in dense urban environments. They asserted that the experiments and numerical results have revealed a slight effect of (SSSI) on the seismic response of the buildings considered in their research. Lu et al. [3] developed simple discrete models for simulating the static and dynamic interaction between multiple buildings. The developed models have been validated by comparison with the results of the simulation methods of FEs and boundary elements (BE). A thorough series of 2D numerical analyses were carried out by Bybordiani and Arici [4] to study the interaction effect between neighboring 5-, 15-, and 30-story clusters of structures and the surrounding viscoelastic half-space. They investigated the influence of the inter-building distance and the foundation material on the response of the adjacent buildings. The results revealed negligible effects of (SSSI) on the behavior of the identical low-rise structures and significant effects on the response of the identical high-rise structures. In the same manner, Isbiliroglu et al. [5] conducted parametric numerical analyses to study the effects of (SSSI) for various arrangements of regular building clusters composed of three types of buildings of approximately 3, 13, and 40 stories. The results pointed out to considerable drop in buildings base motion at frequencies above the natural frequencies of the building foundation systems. Likewise, both detailed numerical analyses and a set of centrifuge experiments have been employed by Bolisetti and Whittaker [6] to investigate the effect of (SSSI) on three arrangements of low- to medium-rise frame buildings. They concluded that the existence of deep vault reduces uplift in the foundations and the peak spectral accelerations at the roof. Ogut [7] has conducted a wide (SSSI) analytical parametric study; the effects of mass, height of the superstructures, foundation types, embedment situations, and natural frequencies of two and three closely spaced buildings on (SSSI) have been investigated. By studying the (SSSI) effect on 32-story neighboring buildings for different inter-building spacings, Yahyai et al. [8] claimed a detrimental effect of (SSSI) on base shear forces and lateral displacement. Also, detailed numerical analyses for obliquely incident seismic waves were carried out by Álamo et al. [9]. They noted that the inter-building spacing and the seismic loading are crucial for the (SSSI) effects on short identical structures supported by pile foundations. In a related study, Rahgozar [10] has employed the direct method for evaluating the behavior of 3D FE models of neighboring 15- and 30-story steel structures founded on different sandy and clayey soils. The results demonstrated the detrimental effect of (SSSI) for the case of neighboring tall

buildings to short buildings. Nakamura et al. [11] conducted a comprehensive seismic analysis by using a nonlinear 3D FE model to determine the (SSSI) and the ground irregularity effect on the seismic response of nuclear power plants (NPPs). Roy et al. [12] performed a detailed parametric study to analyze the impact of (SSSI) on the behavior of neighboring light structure to a heavy structure, and a heavy structure adjacent to a heavy structure for several soil cases, foundation embedment depths, and separation distances. The results asserted that the SSSI response of light or heavy structures can be influenced by the existence of nearby heavy structures. Barrios and Chouw [13] performed a physical experimental study by using a sand-filled laminar box on a shaking table. The examined adjacent structures had identical mass and different fundamental periods. They concluded that the buildings with lower natural frequencies are less vulnerable to the (SSSI) effect than the buildings with higher natural frequencies. Ikeda et al. [14] conducted a comprehensive analytical and numerical study on the (SSSI) effect among multiple foundations (without superstructures). Larkin et al. [15] performed shaking table tests with a laminar box for four neighboring buildings. They denoted that the (SSSI) effects are more evident for neighboring structures with different fundamental frequencies due to the mechanism of energy exchange between them. Ge et al. [16] conducted comprehensive experimental tests and numerical studies to investigate the (SSSI) effect between multiple high-rise buildings. The results revealed beneficial effect of (SSSI) on the acceleration responses of structures and adverse effect on the structures' deformations. Furthermore, two centrifuge tests were performed by Trombetta et al. [17] to assess the (SSSI) effects between midrise elastic shear wall buildings supported by a mat foundation and low-rise inelastic frame buildings built on individual spread footings. Andersen et al. [18] extended the validity of a semi-analytical model predicting ground vibration from rigid rectangular loads to enable it to estimate accurately the effect of heavy masses or plates set either on the ground surface or implanted into the soil. Similarly, Gan et al. [19] carried out thorough numerical analyses of the (SSSI) effect between three adjacent structures supported by pile-raft foundations embedded in viscoelastic half-space. The results revealed that the (SSSI) impact depends mainly on the structural characteristics, rather than the location of the structures. Wang [20] employed the FE software (ANSYS) to analyze the (SSSI) effect between the surface structure built on viscoelastic soil layer and the adjacent underground station. The results denoted that the arrangement and the fundamental frequencies of the

structures have crucial impact on the (SSSI) effect. Bard et al. [21] conducted extensive experimental, numerical, and theoretical cross-analyses to quantify multi-building interactions (SSSI) and site-city effect. An idealized experimental model of a city on a soft layer has been used to examine the effect of multiple SSSI. Schwan et al. [22] performed a set of shake table tests on a designed elementary case study of multiple (SSSIs) between clusters of structures. The experimental data were compared with theoretical and numerical results. They demonstrated experimentally, theoretically, and numerically the fact that a city group effect can significantly alter the seismic response of both the construction site and the related buildings; also, they quantified the complex (SSSIs) at the city scale. Mason et al. [23] conducted centrifuge tests on two adjacent moment-resisting frame steel structures. The first model structure is a one-story, lumped-mass frame structure based on embedded spread footings. The other model structure is a three-story, lumped-mass frame structure founded on a one-story aluminum basement. A comprehensive set of dynamic geotechnical centrifuge tests was carried out by Ngo et al. [24] to investigate the (SSSI) effects on the behavior of two adjacent structures with different mass, natural frequency, and height. Extensive numerical analyses were conducted by Alam and Kim [25] to explore the effect of uniform and nonuniform ground motions on the behavior of neighboring reinforced concrete (RC) frame structures. The results revealed a remarkable impact of the spatial variation of ground motions on the seismic response of the adjacent structures. Ritter [26] employed a novel 3D technology to investigate the (SSSI) effect between a tunnel, the soil, and existing structures. The building models were printed with brittle material behavior similar to masonry and tested in a geotechnical centrifuge. A thorough series of numerical analyses were conducted by Alfach [27] to examine the effect of the plan positioning of bridges toward the seismic excitation direction and inter-bridge spacing of three dissimilar adjacent bridges supported by a group of piles embedded in nonlinear clay. Knappett et al. [28] examined the seismic performance of an isolated structure and adjacent (similar and dissimilar) structures under a series of strong seismic excitations. The nonlinear dynamic centrifuge tests were accurately validated by a comprehensive nonlinear FE model. Furthermore, Ada et al. [29] investigated the (SSSI) effect between two neighboring frame structures through a series of 3D numerical analysis. They examined the influences of the stiffness of the underlying soil, layout of the structures, the clear distance between the structures, and the number of stories of the structures. They

concluded that the (SSSI) effect depended highly on the dynamic characteristics of the adjacent structures. Vicencio et al. [30] have discussed the pros and cons of the leading developments of (SSSI) and site-city interaction (SCI) effects with focusing on the theoretical idealization of SSSI by means of low-fidelity models with comparable predictive accuracy. Ghasemzadeh and Alibeikloo [31] developed a simple analytical solution for computing the dynamic interaction tensor for floating pile groups with batter piles. The governing differential equations were derived for an unloaded batter floating pile closely spaced to another loaded pile with the same properties. Asgarian et al. [32] studied the dynamic response of pile-supported structures by comparing the experimental and numerical dynamic responses of a prototype jacket offshore platform. Ghasemzadeh et al. [33] examined the effects of batter angle, slenderness ratio, spacing between piles, pile-soil stiffness ratio, and soil plasticity on pile-soil-pile interaction factors.

1.1 Aims

The main objective of this paper is developing better understanding of SSSI between three dissimilar bridges with different superstructure mass ratios. Notably, the contents of this study focused on the effect of inter-bridge spacing and dissimilar bridge geometrical arrangements on the (SSSI) impact. In this paper, we enlarge the range of our former studies about the (SSSI) effect between two identical bridges in Alfach and Al Helwani [34] and the (SSSI) effect between two dissimilar bridges in Alfach [35] to study the case of three dissimilar bridges with different superstructure mass ratios. The numerical analyses were performed using a finite difference modeling software fast Lagrangian analysis of continua in three dimensions (FLAC 3D). The analyses have been undertaken for nonlinear clay.

More specifically, the research contributions in assessing the effect of SSSI could be summarized in these three points:

- identification of the nature of (SSSI) effect (detrimental, constructive, or neutral) between three adjacent dissimilar bridges with different superstructure ratios;
- exploring the impact of inter-bridge spacing on the seismic performance of the neighboring bridges; and
- investigation of the seismic efficiency of the planned alignment of adjacent structures with respect to each other and the epicentral direction (parallel, perpendicular, crossing).

2 Numerical model of adjacent bridges

2.1 Soil–pile–bridge model

The (SSSI) system in this study consisted of three asymmetric RC bridges. These bridges of lumped masses of 350, 700, and 1050 t have been used for forming different neighborhood combinations. The used bridges were supported by floating pile groups of six, 12, and 18 piles, respectively, for the purpose of retaining the single pile static axial load to 80 t. The fixed-head pile groups were embedded into homogeneous nonlinear cohesive layer ($C = 150$ kPa, $\varphi = 0$) underlined by rigid bedrock as shown in Figure 2. The soil behavior was simulated based upon the standard Mohr–Coulomb

criterion through an elastoplastic law without hardening. Table 1 presents the essential geotechnical characteristics of the soil layer. The length and diameter of the piles are $L_p = 10.5$ m and $D_p = 0.8$ m, respectively. The piles are connected rigidly by an RC cap of 1 m thickness as illustrated in Figure 1. The compartment of the material of the structural elements (superstructure mass, bridge pillar, cap, and piles) has been defined as elastic. Tables 2 and 3 list the fundamental parameters of the superstructure and the pile groups, respectively.

In light of the high complexity of the subject of SSSI, a set of measures have been adopted:

- Aiming to minimize the computational cost, the soil mesh density was decreased with increase of the distance from the soil center, where the major effect of (SSSI) could take place as shown in Figure 2.
- The absorbent boundaries were employed to avoid the seismic wave's reflection on the structure's model zone.
- To prevent the potential soil–cap interaction, the cap was based at 0.5 m over the soil surface.
- To preclude the possible pile–pile interaction, the inter-pile distance was taken as $S = 3.75 D_p = 3$ m.

To reduce the computation cost and enhance the numerical stability of the analyses, slight damping of Rayleigh type is used for the soil and the structure. A 0.02 damping ratio is used for the structural elements [36] and 0.05 for the soil. The damping of the system could be assumed as Rayleigh damping, where

$$C = \alpha M + \beta K \quad (1)$$

$$\xi_n = \frac{\alpha}{2} \frac{1}{\omega_n} + \frac{\beta}{2} \omega_n \quad (2)$$

C , M , and K are the damping, mass, and stiffness matrices, respectively. α and β are the mass ξ_n proportional coefficient

Table 1: Properties of cohesive soil.

ρ_s (kg/m ³)	E_{os} (MPa)	ν_s	K_o	ζ_s (%)	C (kPa)	φ (°)	Ψ (°)
1700	8	0.3	0.5	5	150	0	0

Table 2: Elastic characteristics of the superstructure.

ρ_{st} (kg/m ³)	E_{st} (MPa)	ν_{st}	ξ_{st} (%)	Mass (t)
2500	8000	0.3	2	350

where ρ_{st} , E_{st} , and ν_{st} are the density, Young's modulus, and the coefficient of Poisson's ratio, respectively. ξ_{st} is the percentage of critical damping, D_p is the pile diameter, and EA and EI are the axial and bending stiffness, respectively.

Table 3: Elastic characteristics of the pile materials.

Material	Diameter (m)	Mass density ρ (kg/m ³)	Young's modulus E (MPa)	Poisson's ratio ν	Damping ratio ξ (%)	Height (m)
Pile	0.8	2500	20,000	0.3	2	10

and stiffness proportional coefficient, respectively. ξ_n is the damping ratio and ω_n is the natural frequency of the structure.

The superstructure was simulated by lumped masses at the top of the pillars $M_{st} = 350, 700, \text{ and } 1050$ t. The flexural stiffness of the superstructure was $K_{st} = 86,840, 1,389,440, \text{ and } 1,389,440$ kN/m respectively, and its fundamental frequencies (assuming a fixed base) were equal to $F_{st} = 2.5, 7.09, \text{ and } 5.78$ Hz, respectively. The latter were computed by using the subsequent formulations:

$$f_{st} = \frac{1}{2\pi} \sqrt{\frac{K_{st}}{M_{st}}}, K_{st} = \frac{3E_{st}}{H_{st}^3} \quad (3)$$

where F_{st} is the fundamental frequency, K_{st} is the flexural stiffness of the superstructure, M_{st} is the lumped mass at the top of the pillar, E_{st} is the elastic modulus of the lumped mass, and H_{st} is the height of the superstructure.

The fundamental frequency of the soil layer is 3.2 Hz. The flexible base frequencies of the superstructure were calculated (using numerical methods) as $F_{st,flex} = 0.827, 0.71, \text{ and } 0.7$ Hz, respectively, taking into consideration the soil–structure interaction.

2.2 Seismic excitation

The numerical analyses have been carried out under the seismic record of the Kocaeli earthquake ($M_w = 7.4$),

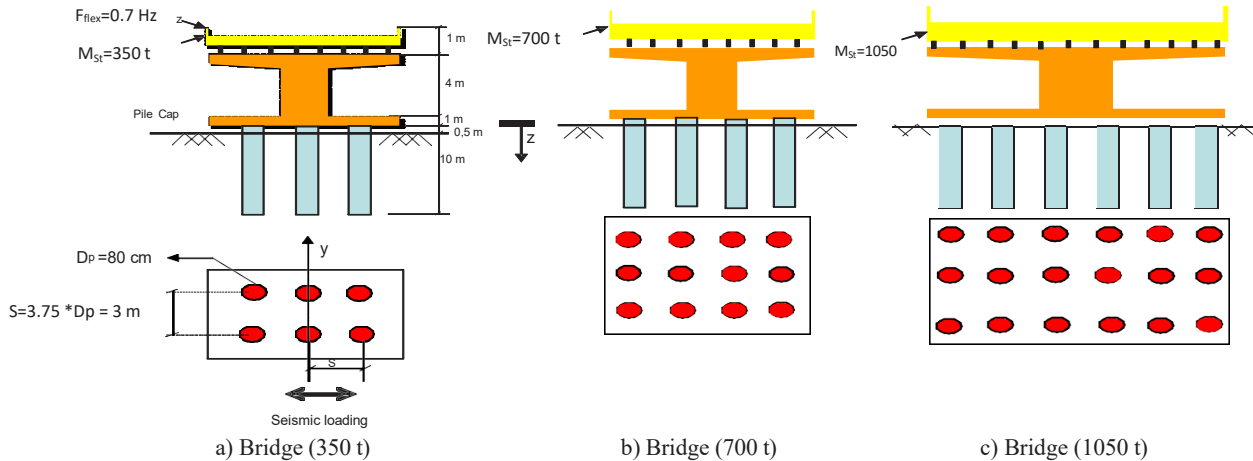


Figure 1: Piles-bridge system geometry.

which occurred on August 17, 1999, in the North Anatolian Fault Zone in Turkey (Station AMBARLI; KOERI source). The peak horizontal acceleration and velocity of this earthquake were Peak Ground Acceleration $PGA = 0.247 \text{ g}$ and $PVA = 40 \text{ cm/s}$, respectively, during the total duration of the record ($t = 30.08 \text{ s}$). Nevertheless, the numerical analyses have been performed for a duration of $t = 8.465 \text{ s}$ to economize the computational capacity and the analyses durations. This step was adopted after rigorous analysis to ensure equalization of the seismic excitation impact for the total duration ($t = 30.08 \text{ s}$) and the used duration ($t = 8.465 \text{ s}$). The seismic loading has applied at the base of the soil under form of velocity. Figure 3 presents the fundamental frequency of the seismic loading ($F = 0.9 \text{ Hz}$) in the Fourier spectrum of the velocity record (Figure 3D). It is worth mentioning that the seismic loading fundamental frequency is between the fundamental frequency of the soil ($F_1 = 3.2 \text{ Hz}$) and the flexible frequency of the structure ($F_{ss} = 0.7 \text{ Hz}$), which justifies the choice of this seismic loading.

2.3 Results and Discussion

Table 4 and Figures 4 and 5 give the results of the bridge with superstructure mass of $M_{st} = 350 \text{ t}$. The results show an important amplification factor at the superstructure mass ($A_{amp} = 10.8$). Furthermore, it is worth noting that the maximal internal forces occurred in the upper and central parts of the piles.

As shown in Figures 6 and 7 and Table 5, the maximum internal forces induced in the piles of the bridge of $M_{st} = 700 \text{ t}$ are smaller by about 25% than those of the piles of the bridge of $M_{st} = 350 \text{ t}$. Furthermore, the amplification factor at the mass was reduced by a ratio of $A_{amp} = 7.95$. Also, it is noteworthy that the bending moment profile has

changed drastically by recording the maximum values at the top parts of the piles.

Finally, the maximum bending moment ($M = 2947 \text{ kN m}$) and the minimum shear force ($T = 623.3 \text{ kN}$) among the three isolated bridges of superstructure masses ($M_{st} = 350, 700, 1050 \text{ t}$) were obtained for the bridge of mass $M_{st} = 1050 \text{ t}$ as shown in Figures 8 and 9. In addition, the mass and cap accelerations of the bridge of mass $M_{st} = 1050 \text{ t}$ have dropped sensibly to 11.99 and 10.82, respectively, as presented in Table 6. Likewise, the amplification factor of the mass has decreased to $A_{amp} = 5.64$.

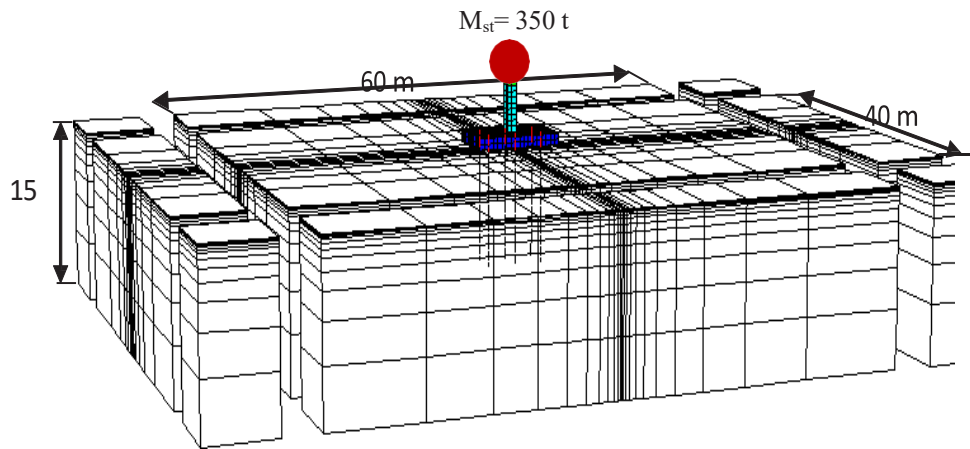
3 Bridge-Soil-Bridge System

The following numerical simulations have been carried out for several configurations of three dissimilar bridges for two superstructure mass ratios (200% and 300%). The impact of two essential factors has been examined: 1) inter-bridge spacing and 2) the geometric position of neighboring structures toward each other and the seismic loading direction (parallel, perpendicular, crossing) configurations for the above-stated mass ratios.

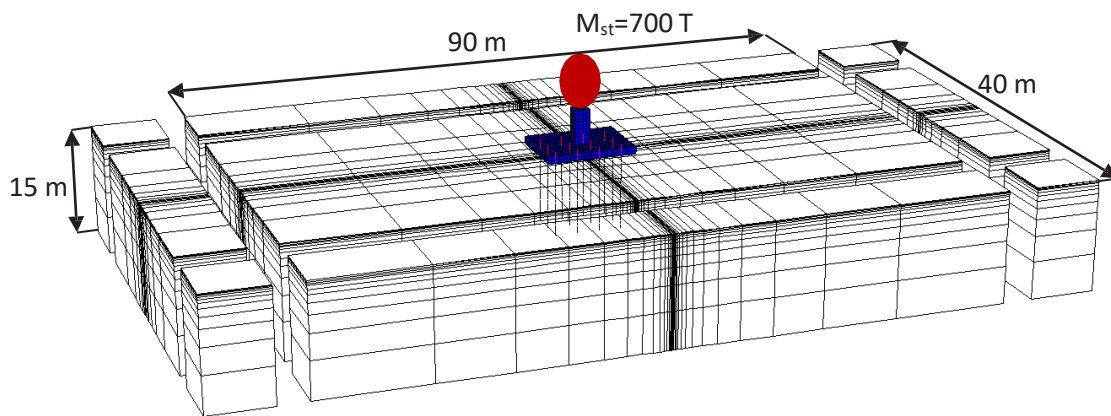
3.1 Three bridges with superstructure mass ratio (200%)

3.1.1 Effect of inter-bridge spacing

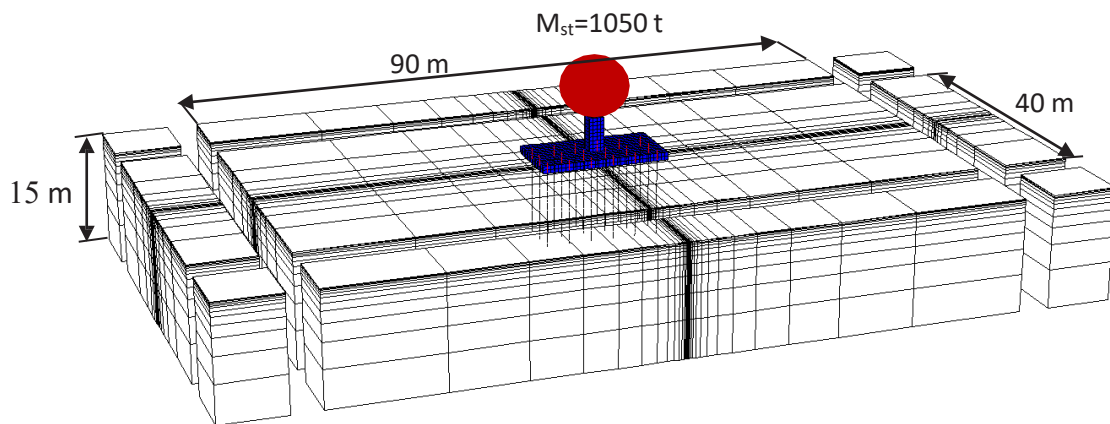
The effect of inter-bridge spacing on the (SSSI) effect between three different parallel bridges has been numerically analyzed; the central bridge is the heavier one with a superstructure mass of $M_{st} = 700 \text{ t}$ (Figure 2b) located



a) Bridge (350 t) – 3D numerical mesh (138 structural elements and 6978 nodes)

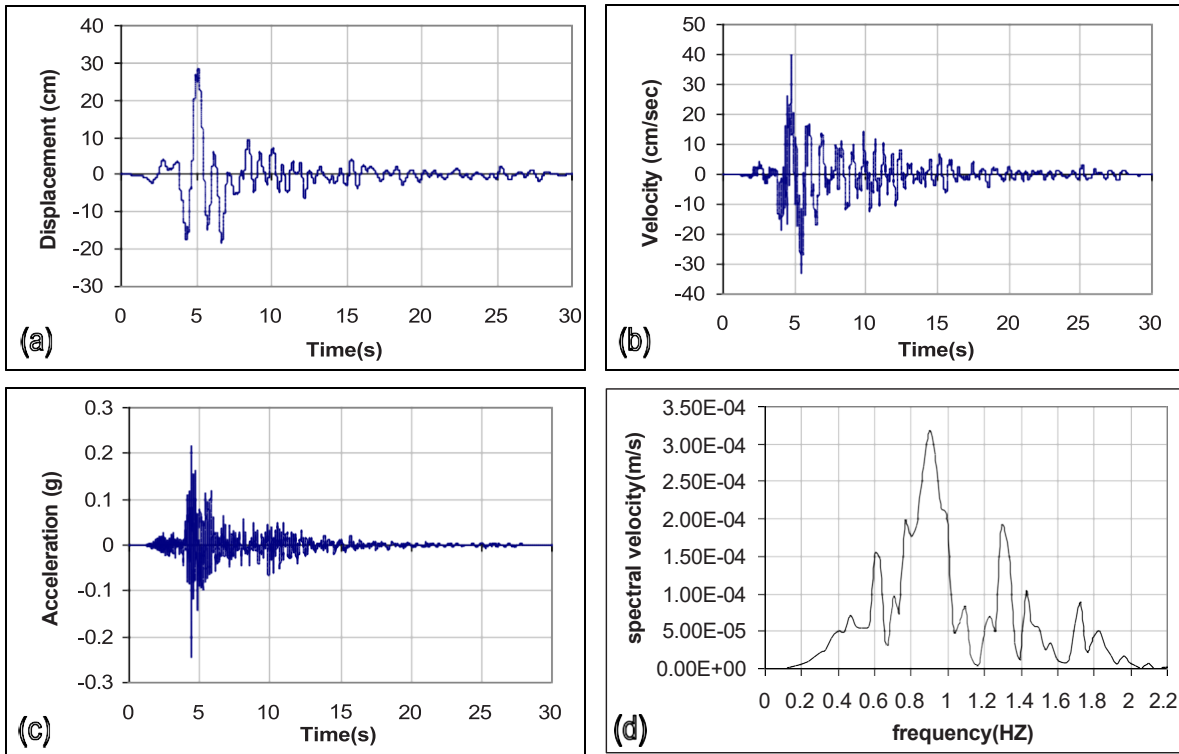


b) Bridge (700 t) – 3D numerical mesh (276 structural elements and 10,086 nodes)



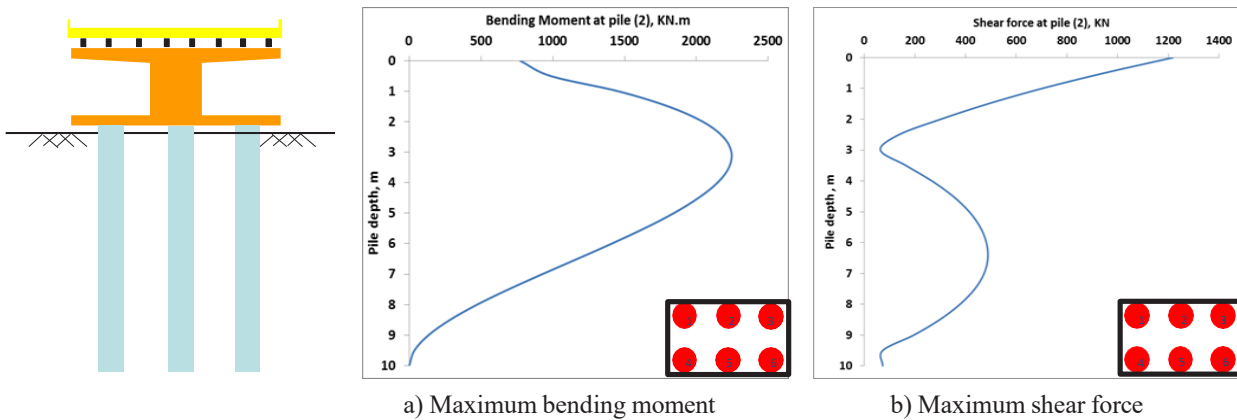
c) Bridge (1050 t) – 3D numerical mesh (414 structural elements and 10,656 nodes)

Figure 2: 3D numerical mesh of soil–piles–bridge system.



a) Displacement, b) velocity, c) acceleration, d) Fourier spectra of velocity component

Figure 3: Kocaeli earthquake record (1999).



a) Maximum bending moment

b) Maximum shear force

Figure 4: Internal forces at central pile (2).

Table 4: Response of a group of (2 × 3) piles for Kocaeli earthquake (1999).

C Cohesion (kPa)	a_{st} (m/s^2)	a_{cap} (m/s^2)	Internal forces			
			Central piles		Corner piles	
			M_{max} Bending moment (kN m)	T_{max} Shear force (kN)	M_{max} Bending moment (kN m)	T_{max} Shear force (kN)
150	23.02	14.39	2244	1218	2189	1604

a_{st} : acceleration of the superstructure

a_{cap} : acceleration of the cap

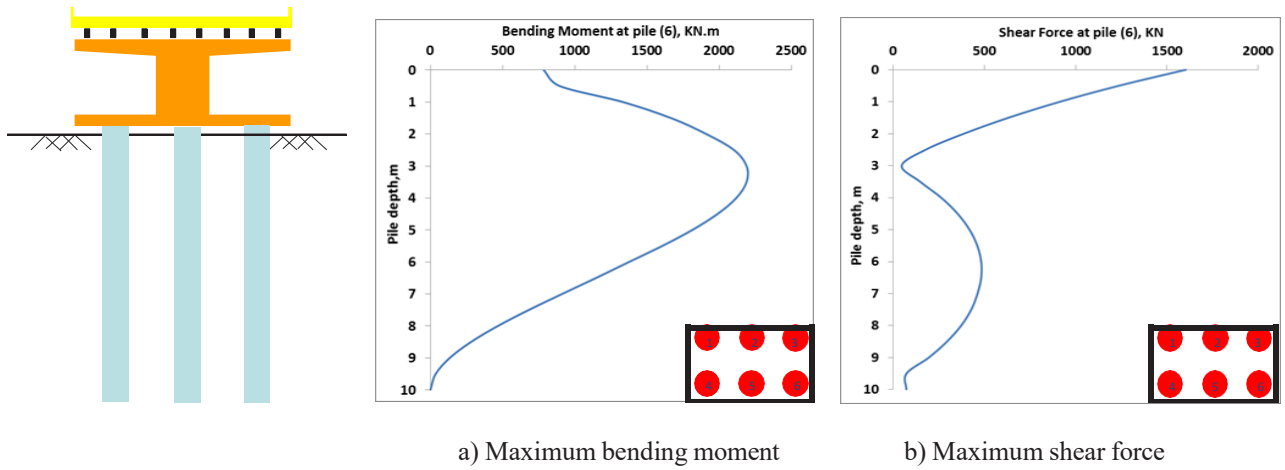


Figure 5: Internal forces at corner pile (6).

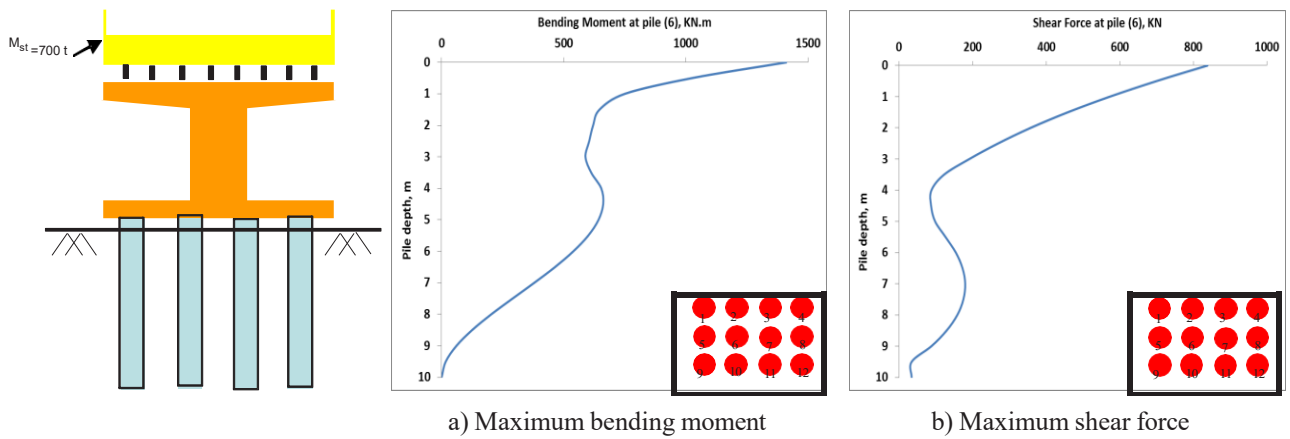


Fig. 6 Internal forces at central pile (6).

Figure 6: Internal forces at central pile (6).

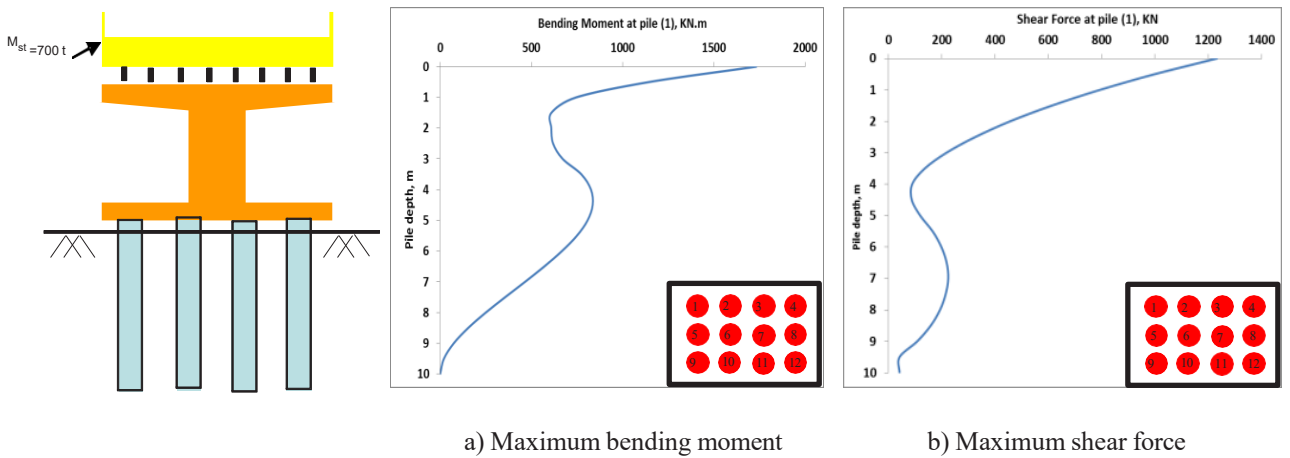


Figure 7: Internal forces at corner pile (1).

Table 5: Response of a group of (4x3) piles for Kocaeli earthquake (1999).

C (kPa)	a_{st} (m/s ²)	a_{cap} (m/s ²)	Internal forces			
			Central piles		Corner piles	
			M_{max} (kN m)	T_{max} (kN)	M_{max} (kN m)	T_{max} (kN)
150	18.09	14.9	1411	837.8	1732	1233

Table 6: Response of a group of (6x3) piles for Kocaeli earthquake (1999).

C (kPa)	a_{st} (m/s ²)	a_{cap} (m/s ²)	Internal forces			
			Central piles		Corner piles	
			M_{max} (kN m)	T_{max} (kN)	M_{max} (kN m)	T_{max} (kN)
150	11.99	10.82	2363	623.3	2947	1007

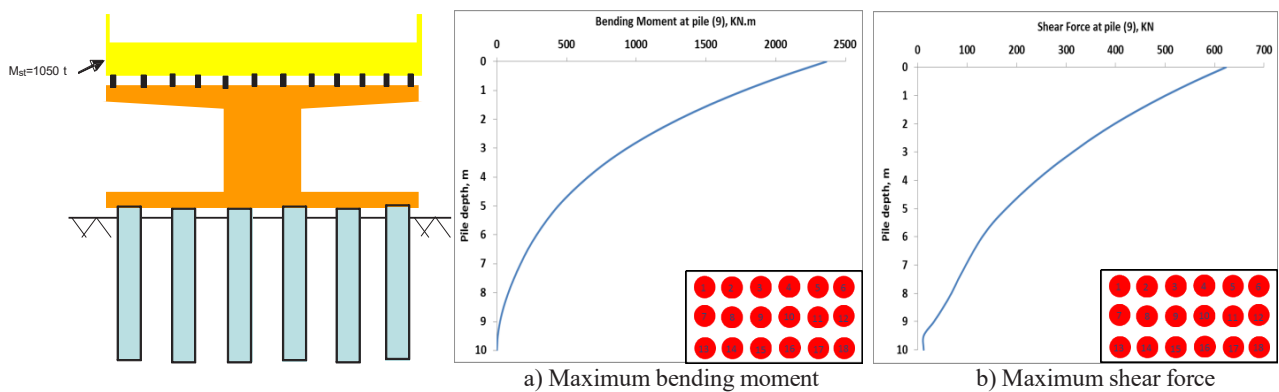


Figure 8: Internal forces at central pile (9).

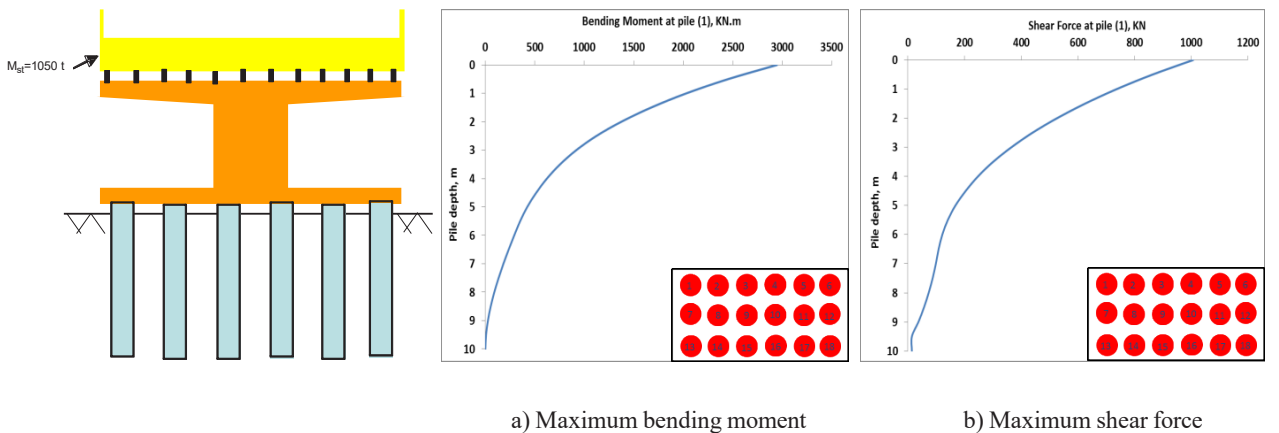


Figure 9: Internal forces at corner pile (1).

between two lighter bridges with a superstructure mass of $M_{st} = 350$ t (Figure 2a). The numerical calculations were undertaken for a range of distances between the bridges, precisely $S = 20, 30,$ and 40 m. All the geometrical and mechanical characteristics of soil and concrete mentioned in section 2.1 and Tables 1–3 have been adopted in these

analyses. The numerical simulation is performed for the seismic loading of the Turkey earthquake (Kocaeli, 1999). The applied mesh presented in Figure 10 includes 4176 zones of eight node solid elements and 552 3D structural elements of two node beam elements.

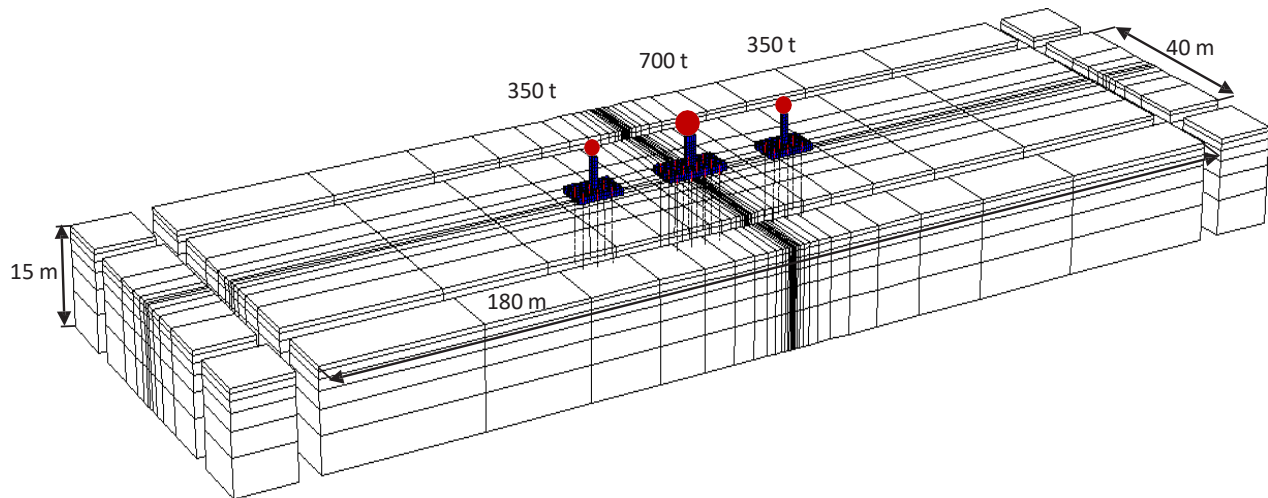


Figure 10: Parallel bridges system 3D numerical mesh with adsorbing boundaries (552 structural elements and 41,361 nodes).

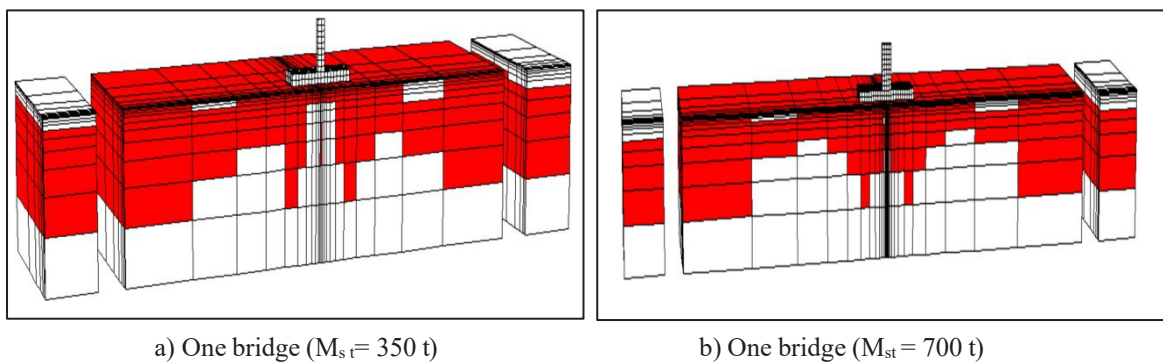


Figure 10: Distribution of plasticity (red zones) for two single isolated bridges ($M_{st} = 350$ and 700 t).

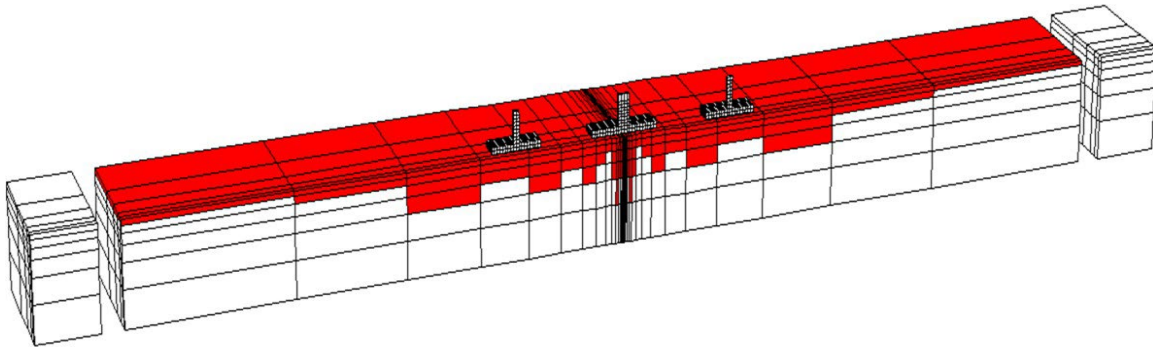
3.1.1.1 Results and Discussion

The spread of plasticity in the soil for the two isolated bridges ($M_{st} = 350$ and 700 t) is presented in Figure 10. Foreseeably, the plasticity extension under the central part of the light bridge ($M_{st} = 350$ t) is much smaller than its peer under the heavy bridge. Likewise, Figure 11 illustrates the plasticity extension for the inter-bridge spacing ($S = 20, 30,$ and 40 m) between three parallel dissimilar bridges under the effect of seismic loading (Kocaeli, 1999).

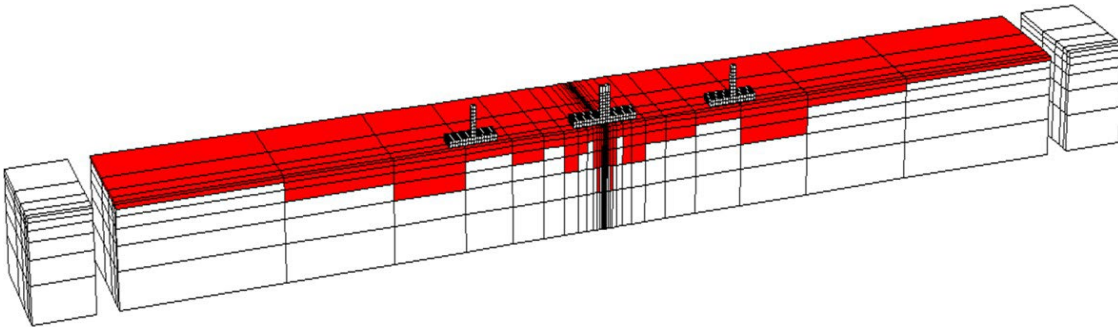
The plasticity spread in the soil has slightly reduced with the increase of inter-bridge spacing as shown in Figure 11. However, plasticity dominated the comportment of the upper part of the soil ($C = 150$ kPa), while the behavior of the lower part stayed mostly elastic because plasticity started at the soil surface and extended gradually toward the base without attaining the base during the seismic loading time.

Table 7 indicates an important positive effect of (SSSI) on both superstructure acceleration and the internal forces induced in the piles. The mass acceleration of the

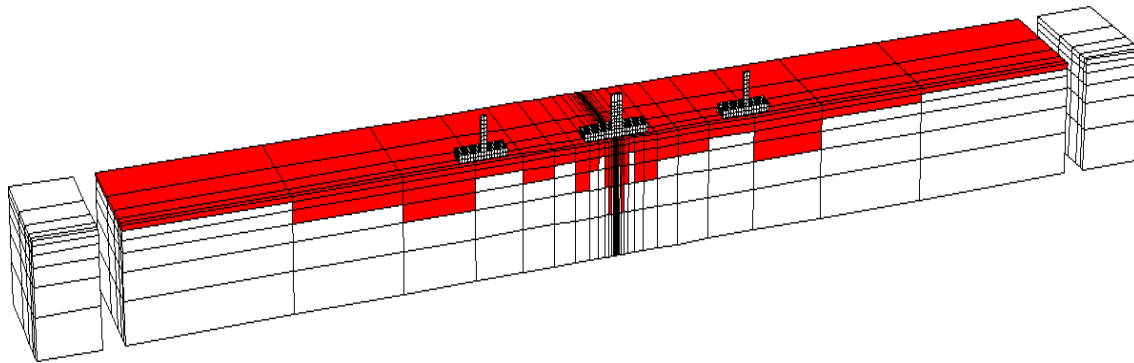
light bridge ($M_{st} = 350$ t) drops sharply (up to 53.28%) due to the (SSSI) effect; similarly, the mass acceleration of the heavy bridge ($M_{st} = 700$ t) decreases by up to 50%. In the same manner, the cap acceleration of the heavy bridge ($M_{st} = 700$ t) and the light bridge ($M_{st} = 350$ t) reduces by up to 61.2%, and 54%, respectively. Regarding the impact of SSSI on the internal forces induced in the piles, the bending moment and the shear force induced in the piles of the heavy bridge ($M_{st} = 700$ t) reduced by up to 31.5% and 12%, respectively, as illustrated in Figures 12 and 13. Similarly, Figures 14 and 15 show a comparable effect of (SSSI) on the piles of the light bridge ($M_{st} = 350$ t) by decreasing the bending moment and the shear force by up to 16.6% and 20.6%, respectively. Hence, the interaction between three dissimilar bridges (SSSI) has valuable positive impacts on the superstructure acceleration and the piles' internal forces by provoking a significant diminution of both. Table 7 and Figures 12–15 demonstrate the slight influence of the inter-bridge spacing on the internal forces provoked in the piles of the three bridges, which is in accordance



a) Three parallel bridges ($S = 20$ m)



b) Three parallel bridges ($S = 30$ m)



c) Three parallel bridges ($S = 40$ m)

Figure 11: Distribution of plasticity (red zones) for different spacings between the three dissimilar bridges ($M_{st} = 350, 700,$ and 350 t).

with the results of Alfach and Al Helwani [34] and Alfach [35] about the minor impact of the inter-bridge spacing. Substantially, the bending moment and the shear force induced in the piles of the light bridge ($M_{st} = 350$ t) increase by up to 6% and 6.9%, respectively, with increase of the inter-bridge spacing. Likewise, the bending moment and the shear force of the heavy bridge ($M_{st} = 700$ t) augment by

up to 4.9% and 6.1%, respectively. In the same manner, the mass and the cap accelerations increase by up to 4.3% and 7.41%, respectively, with increase in inter-bridge spacing as found in Figure 16. It is worth mentioning that all the maximum internal forces induced in the piles have been obtained in the heads of the piles, except the maximum bending moment induced in the piles of the bridge of $M_{st} =$

Table 7: Influence of the spacing inter-bridge on the seismic response of three dissimilar parallel bridges system.

S (m)	ast (m/s ²)		acap (m/s ²)		Internal forces									
							Central piles				Corner piles			
					Pile (2) (Mst = 350 t)		Pile (16) (Mst = 700 t)		Pile (1) (Mst = 350 t)		Pile (7) (Mst = 700 t)			
					Mmax (kN m)	Tmax (kN)	Mmax (kN m)	Tmax (kN)	Mmax (kN m)	Tmax (kN)	Mmax (kN m)	Tmax (kN)		
One bridge (Mst = 350 t and S = 0)	23.02		14.39		2244	1218			2189	1604				
One bridge (Mst = 700 t and S = 0)	18.09		14.9				1640	1134			1732	1233		
S (m)	Bridge (Mst = 350 t)		Bridge (Mst = 700 t)		Three dissimilar parallel bridges									
	ast	acap	ast	acap	Pile (2) (Mst = 350 t)		Pile (16) (Mst = 700 t)		Pile (1) (Mst = 350 t)		Pile (7) (Mst = 700 t)			
20	11.5	6.61	8.45	5.78	1981	1169	1123	998	1824	1310	1218	1090		
30	11.8	6.88	8.63	5.94	2021	1200	1156	1006	1870	1273	1222	1118		
40	12	7.1	8.81	6.05	2035	1242	1176	1037	1935	1361	1278	1157		

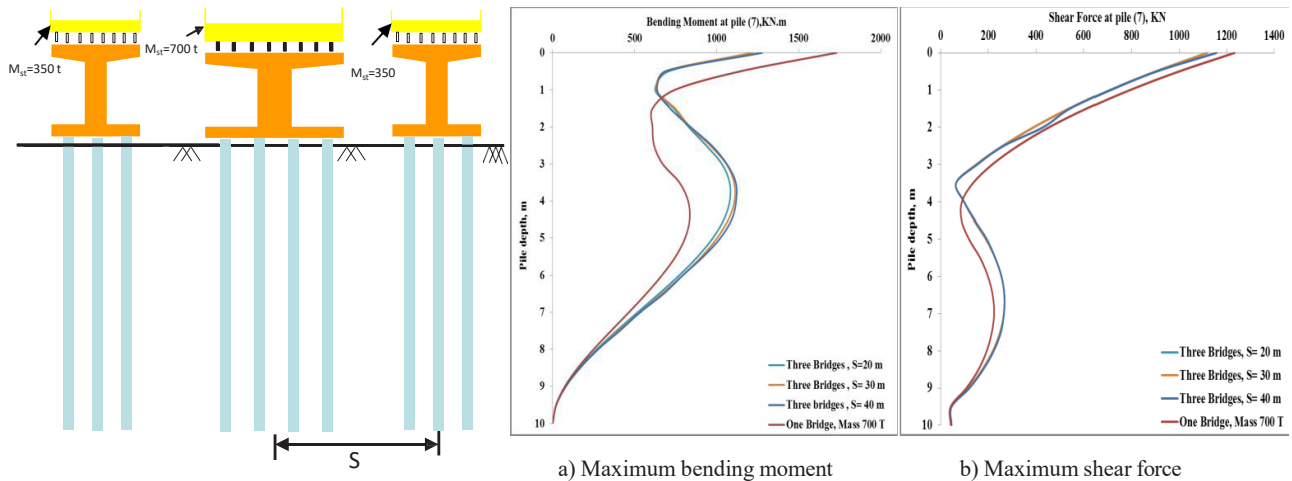


Figure 12: Three dissimilar parallel bridges: Internal forces at corner pile (7) of the bridge (700 t).

350 t, which has been obtained in the central part of the piles as seen in Figures 14 and 15.

In the frequency domain, Figure 17a compares the three dominant frequencies of the mass of the heavy bridge of $M_{st} = 700$ t for the configuration of three adjacent bridges for three inter-bridge spacings ($S = 20, 30,$ and 40 m) with the dominant frequency of the isolated bridge of $M_{st} = 700$ t. The dominant frequency peak ($F = 0.732$ Hz) of the isolated bridge of $M_{st} = 700$ t drops to $F = 0.7$ Hz for the configuration of three neighboring bridges. Likewise, for the light bridge ($M_{st} = 350$ t), Figure 17b shows that the dominant frequency

decreases from $F = 0.709$ Hz for the isolated bridge to $F = 0.6$ Hz for the case of adjacent three bridges for the three aforementioned inter-bridge spacings.

3.1.2 Effect of bridge plan alignment with respect to each other and the seismic loading direction

Three combinations of bridges with respect to the direction of seismic excitations composed of three dissimilar configurations (parallel, perpendicular, and

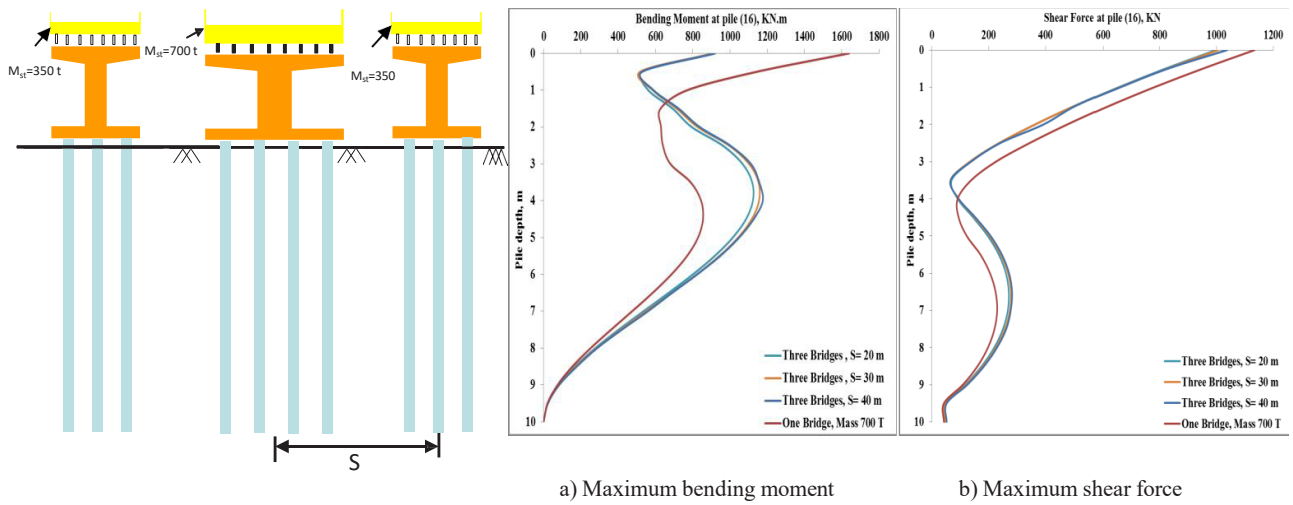


Figure 13: Three dissimilar parallel bridges: Internal forces at central pile (16) of the bridge (700 t).

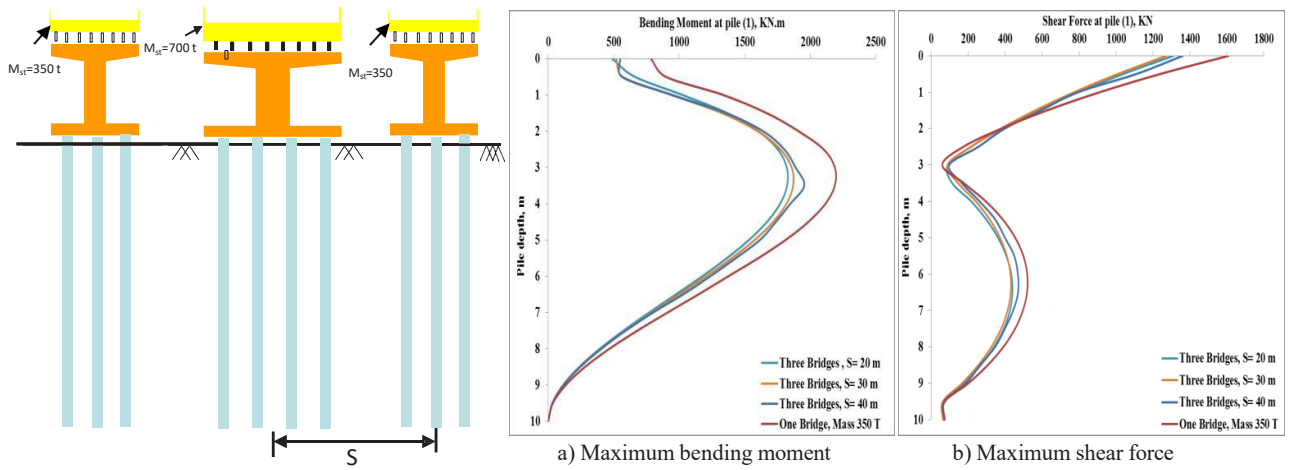


Figure 14: Three dissimilar parallel bridges: Internal forces at corner pile (1) of the bridge (350 t).

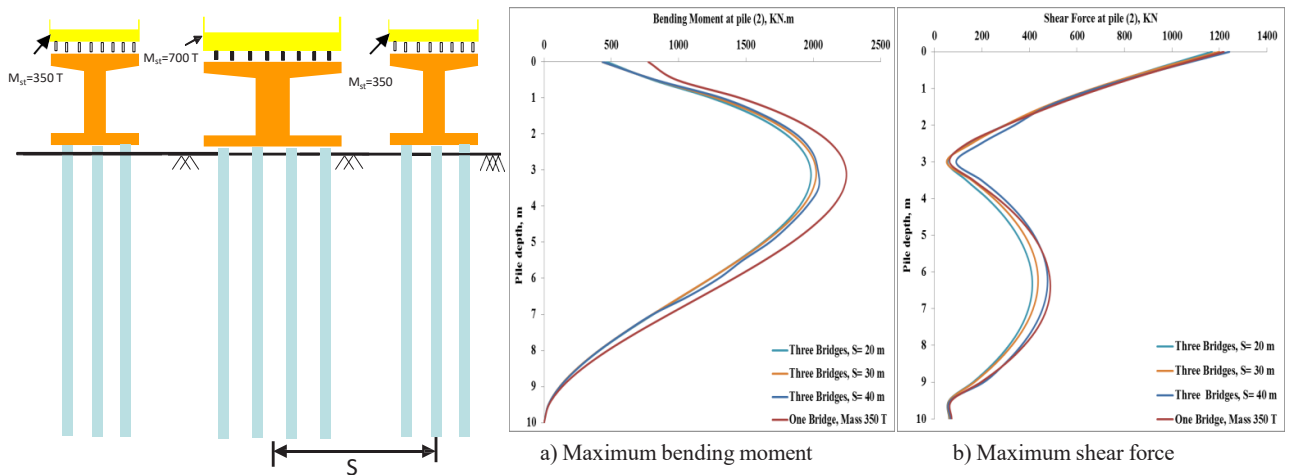


Figure 15: Three dissimilar parallel bridges: Internal forces at central pile (2) of the bridge (350 t).

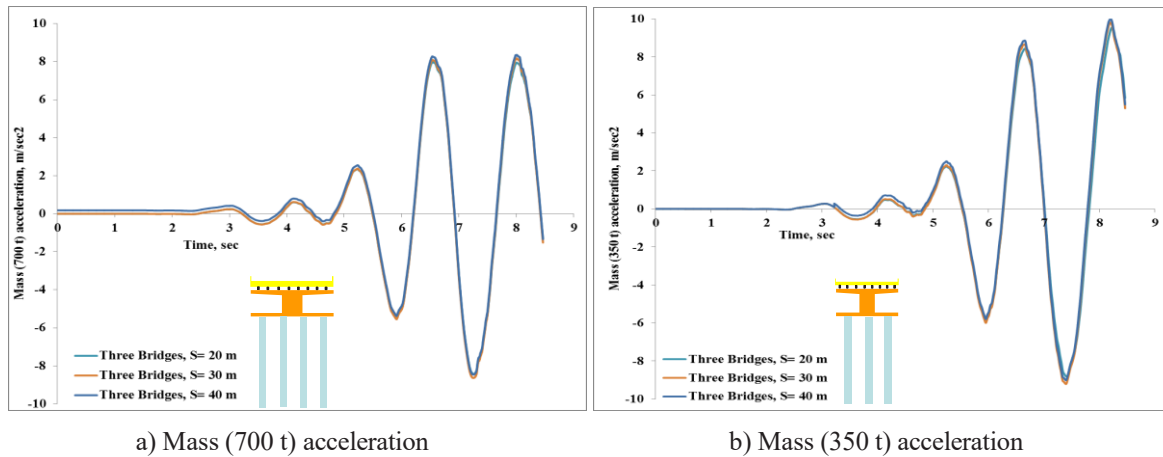


Figure 16: Three dissimilar parallel bridges: Masses accelerations.

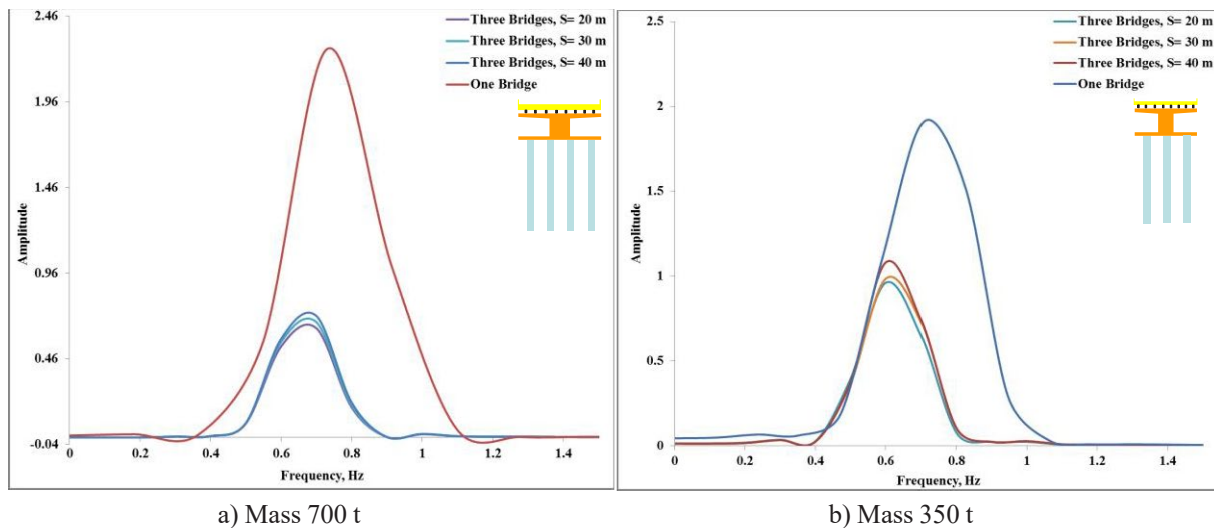


Figure 17: Three dissimilar parallel bridges: Fourier spectra diagram.

crossing) have been considered for the above-mentioned heavy bridge of $M_{st} = 700$ t and light bridge of $M_{st} = 350$ t. An extensive series of numerical calculations were carried out on the three mentioned configurations of parallel, perpendicular, and crossing bridges to evaluate the influence of the direction of the bridges toward each other and toward the seismic loading direction on the (SSSI) effects. The numerical analyses were performed for an inter-bridge spacing of $S = 20$ m and under the seismic record of Turkey (Kocaeli, 1999) presented in Figure 3. Furthermore, the mechanical and geometrical properties shown in Figure 1 and Tables 1-3 have been used in these calculations. The adopted mesh for perpendicular and crossing configurations displayed in Figures 18 and 19, respectively, includes 77,990 nodes and 552 beam structural elements of two nodes.

3.1.2.1 Results and discussion

Figure 20 demonstrates the deep extension of the plasticity under the perpendicular isolated bridge of $M_{st} = 350$ t; differently, the plasticity prolongation was substantially smaller for the heavy isolated bridge of $M_{st} = 700$ t. Similarly, the plasticity prolonged and attained the soil base under the light bridges of $M_{st} = 350$ t and the heavy bridge of $M_{st} = 700$ t reduced significantly for the perpendicular and crossing configurations presented in Figure 21. Nevertheless, the plasticity prolonged and attained the soil base under the heavy bridge of $M_{st} = 700$ t for the crossing bridges' configuration.

Table 8 and Figures 22-26 demonstrate the key constructive role of (SSSI) on the seismic behavior of the neighboring bridges. Both superstructure acceleration and the piles' internal force reduced significantly under

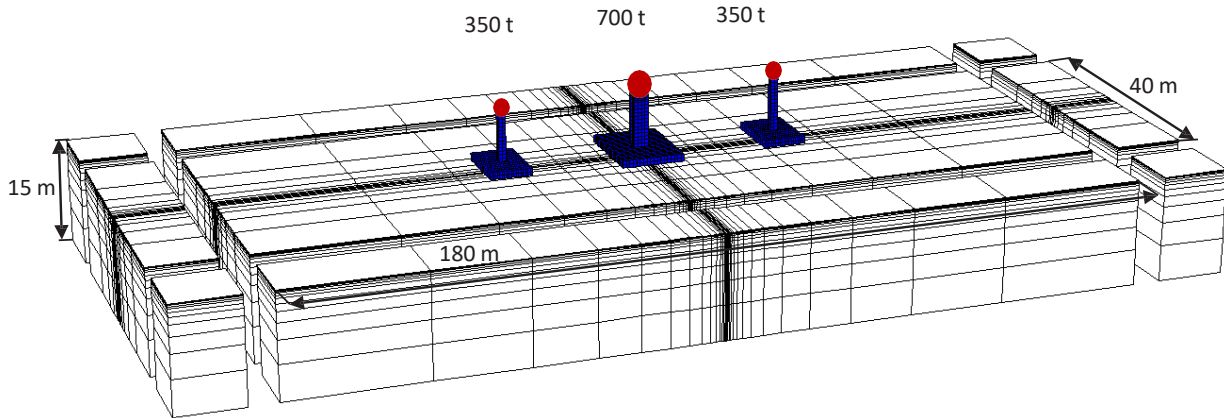


Figure 18: Perpendicular bridges system 3D numerical mesh with adsorbing boundaries (552 structural elements and 77,990 nodes).

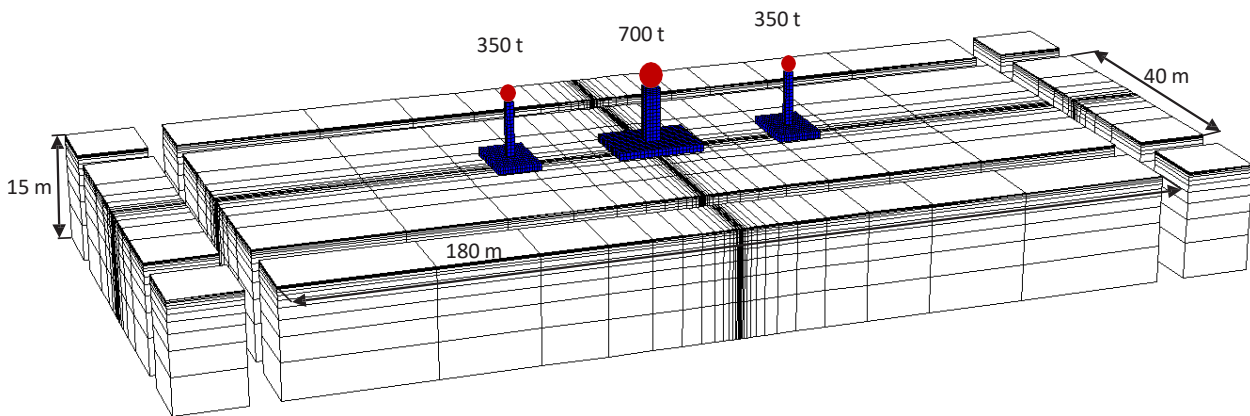
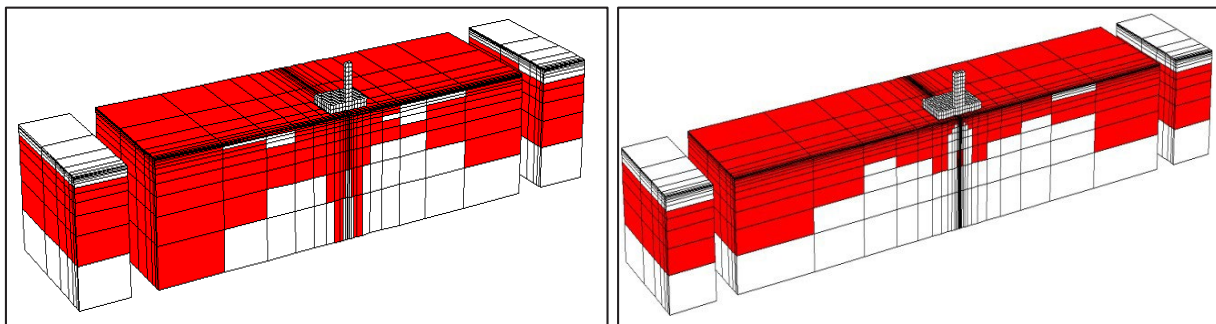


Figure 19: Crossing bridges system 3D numerical mesh with adsorbing boundaries (552 structural elements and 77,990 nodes).



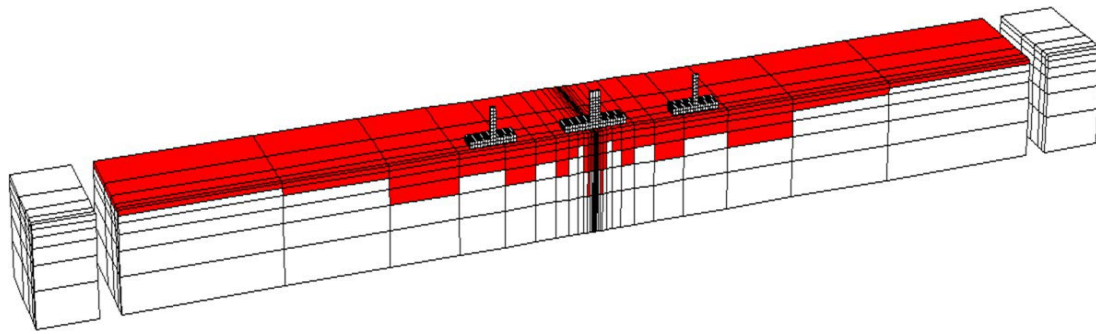
a) One perpendicular bridge ($M_{st}=350$ t)

b) One perpendicular bridge ($M_{st}=700$ t)

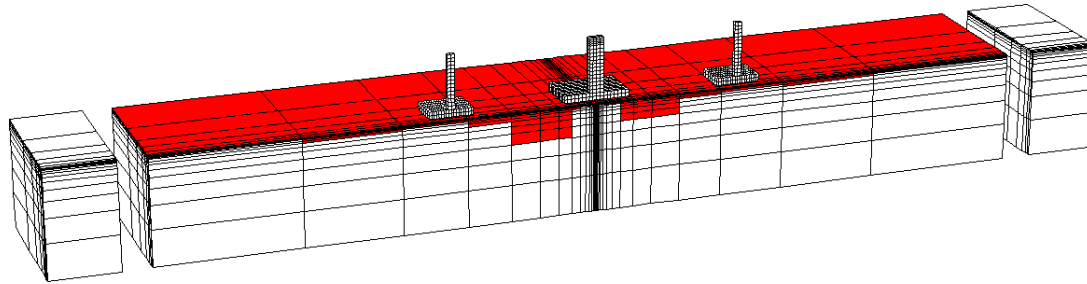
Figure 20: Distribution of plasticity for two single isolated bridges ($M_{st}=350$ and 700 t).

the crucial impact of (SSSI). Concerning the acceleration of the superstructure, the mass and cap accelerations of the light bridge of $M_{st} = 350$ t decreased considerably (up to 42.8% and 42.5%, respectively). Correspondingly, the mass and cap accelerations of the heavy bridge of $M_{st} = 700$ t reduced drastically (by up to 58.8% and

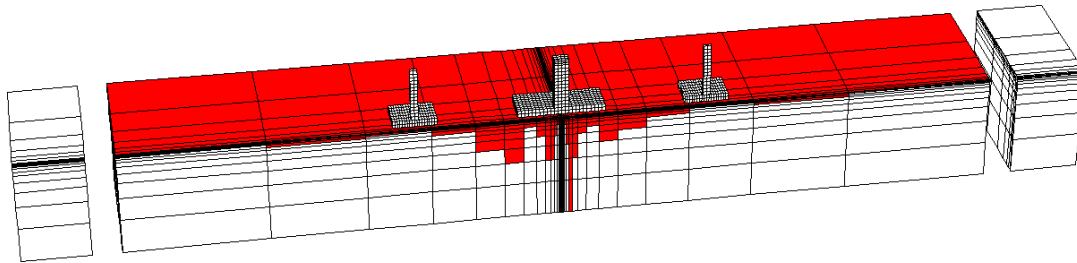
53.72%, respectively). The beneficial impact of (SSSI) on the piles' internal forces was much pronounced through very large reduction of the bending moment and the shear force of the light bridge of $M_{st} = 350$ t by up to 88.49% and 88.7%, respectively. Similarly, but by smaller ratios, the bending moment and the shear force



a) Parallel bridges

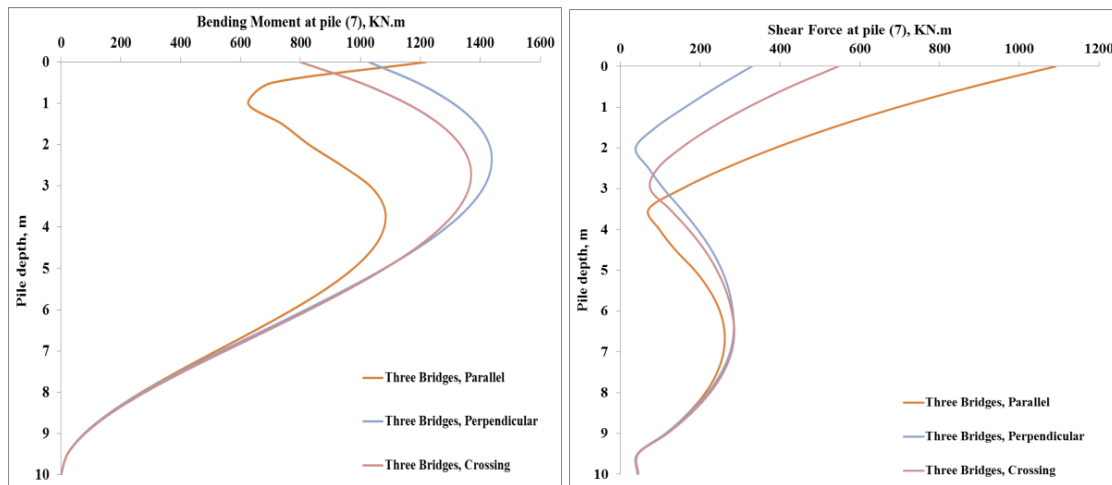


b) Perpendicular bridges



c) Crossing bridges

Figure 21: Distribution of plasticity (red zones) for different positioning of the three dissimilar bridges ($M_{st} = 350, 700, \text{ and } 350 \text{ t}$).



a) Maximum bending moment

b) Maximum shear force

Figure 22: Three dissimilar bridges: Internal forces at corner pile (7) of the bridge (700 t).

Table 8: Influence of different positioning of three dissimilar bridges on the seismic response system.

Position	a _{st} (m/s ²)	a _{cap} (m/s ²)	Internal forces									
			Central piles				Corner piles					
			Pile (2) (M _{st} = 350 t)		Pile (15) (M _{st} = 700 t)		Pile (1) (M _{st} = 350 t)		Pile (7) (M _{st} = 700 t)			
M _{max} (kN m)	T _{max} (kN)	M _{max} (kN m)	T _{max} (kN)	M _{max} (kN m)	T _{max} (kN)	M _{max} (kN m)	T _{max} (kN)					
One perpendicular bridge (M _{st} = 350 t)	20.1	11.5	3979	1268			4093	1330				
One perpendicular bridge (M _{st} = 700 t)	20.53	12.49			2196	1325			2061	1294		
Position	Bridge		Bridge		Three dissimilar bridges							
	(M _{st} = 350 t)		(M _{st} = 700 t)		Pile (2) (M _{st} = 350 t)		Pile (15) (M _{st} = 700 t)		Pile (1) (M _{st} = 350 t)		Pile (7) (M _{st} = 700 t)	
	a _{st}	a _{cap}	a _{st}	a _{cap}								
Parallel	11.5	6.61	8.45	5.78	1981	1169	1218	1090	1890	1309	1218	1090
Perpendicular	0.54	6.52	1.83	1.44	501.9	155.4	1508	363.1	490.4	161.2	1438	328.6
Crossing	0.53	6.47	2.46	1.34	457.8	143.2	1367	545	478.7	159.6	1367	545.2

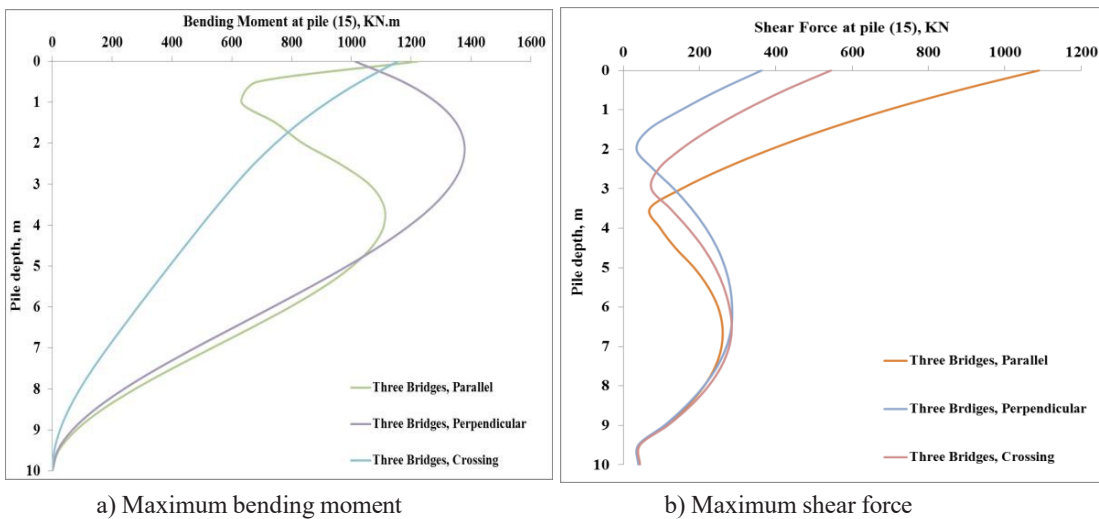


Figure 23: Three dissimilar bridges: Internal forces at central pile (15) of the bridge (700 t).

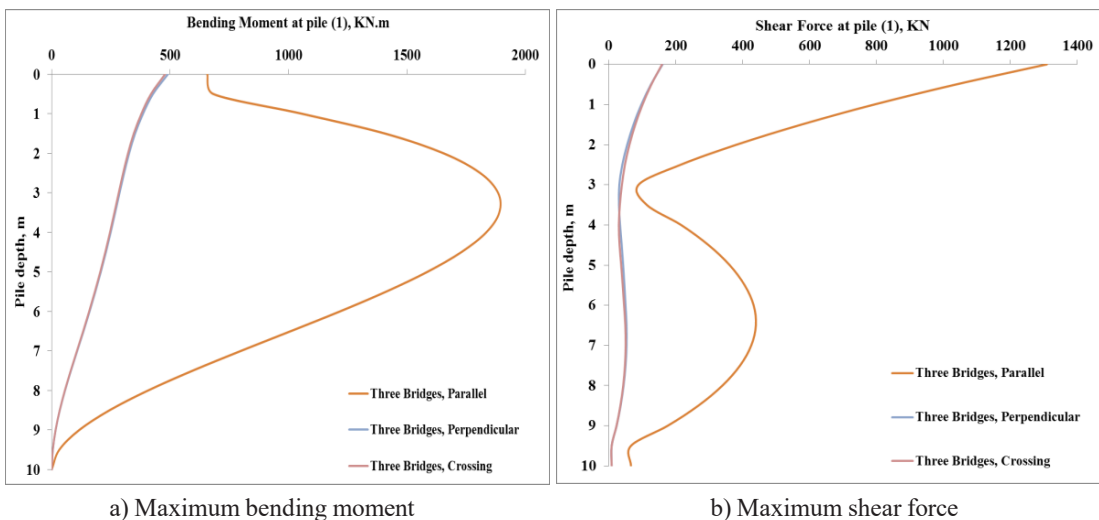


Figure 24: Three dissimilar bridges: Internal forces at corner pile (1) of the bridge (350 t).

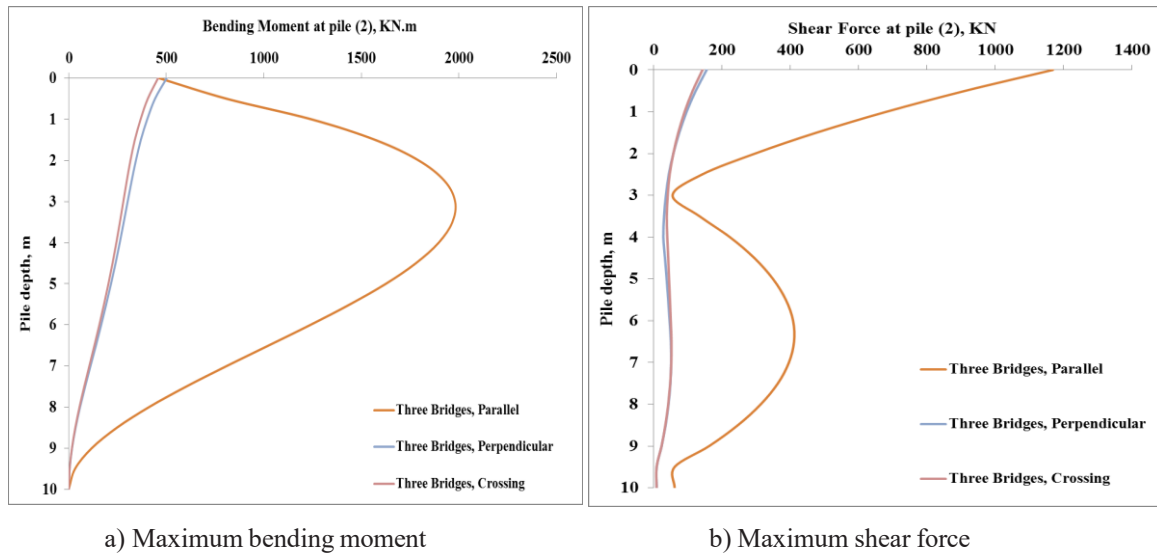


Figure 25: Three dissimilar bridges: Internal forces at central pile (2) of the bridge (350 t).

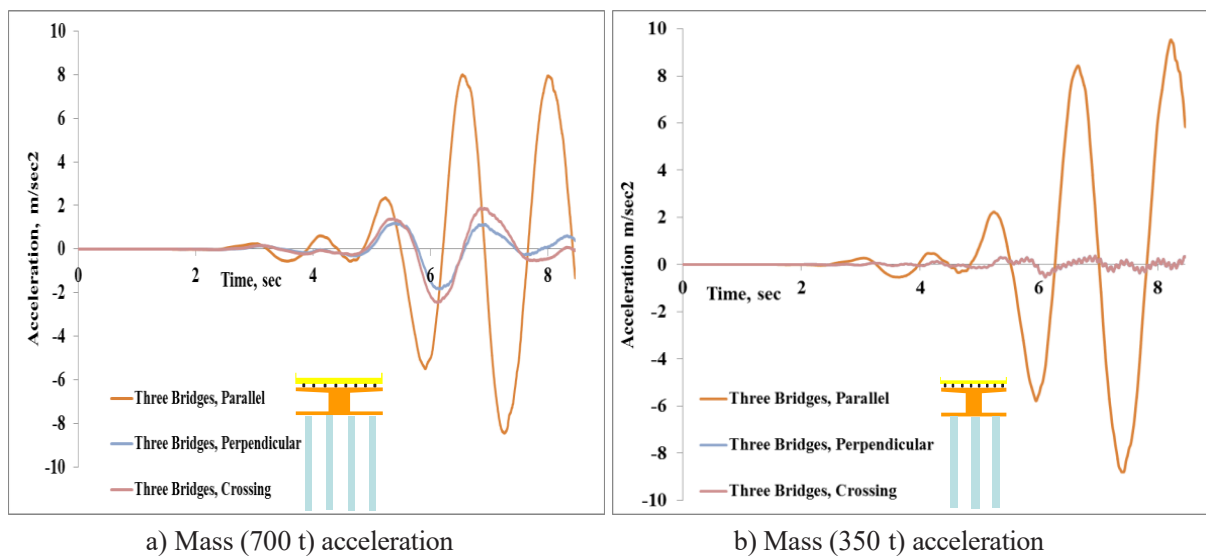


Figure 26: Three dissimilar bridges: Masses accelerations.

of the heavy bridge ($M_{st} = 700$ t) dropped by up to 44.53% and 74.2%, respectively.

In terms of the pile's internal forces, the minimum bending moments induced in piles (1) and (2) of the light bridge of $M_{st} = 350$ t were reported in the configuration of crossing bridges with $M_{min1} = 478.7$ kN m and $M_{min2} = 457.8$ kN m accompanied by the minimum shear forces ($T_{min1} = 159.6$ kN and $T_{min2} = 143.2$ kN) as found in Figures 24 and 25. Moreover, the internal forces induced in piles (1) and (2) were very close for the configurations of perpendicular and crossing bridges as shown in Table 8 and Figures 24

and 25. Conversely, the maximum bending moment and shear force induced in piles (7) and (15) of the heavy bridge ($M_{st} = 700$ t) were reported for the perpendicular bridge configuration. However, the minimum bending moment and shear force in the piles (7) and (15) were noted in the case of parallel bridges as shown in Figures 22 and 23. It is noteworthy that the minimum accelerations in the superstructure elements (mass [$A_{st} = 0.53$ m/s²] and cap [$A_{cap} = 6.47$ m/s²]) have been observed in the case of crossing bridge configuration for the light bridge of $M_{st} = 350$ t as depicted in Figure 26.

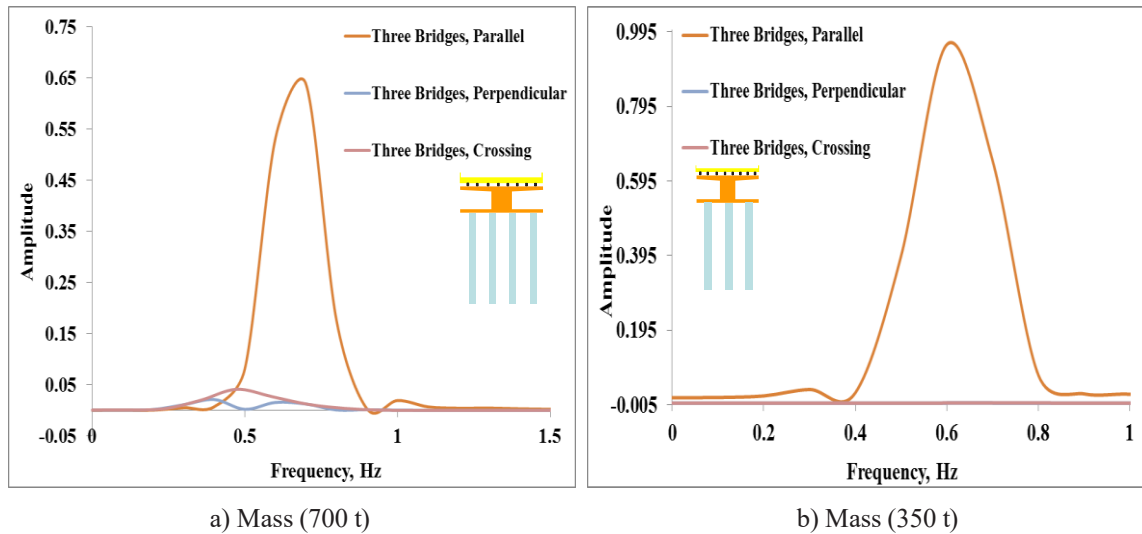


Figure 27: Three dissimilar bridges: Fourier spectra diagram.

Similarly, the best impact of (SSSI) on the cap acceleration was noted for the minimum cap acceleration of the heavy bridge of $M_{st} = 700$ t, which attained $A_{cap} = 1.34$ m/s² for the configuration of the crossing bridges, agreeing with the conclusions obtained by Alfach and Al Helwani (2019) and Alfach (2021). However, the minimum acceleration in the mass of the heavy bridge of $M_{st} = 700$ t was obtained for the perpendicular configuration with $A_{st} = 1.83$ m/s² as shown in Figure 26a. It is pertinent to note that the perpendicular and crossing configurations have an uncommon impact on the vibration of the superstructure of the light bridge of $M_{st} = 350$ t, which was represented by generating bigger accelerations in the cap by $A_{cap} = 6.52$ and 6.47 m/s² accompanied by much smaller accelerations in the mass ($A_{st} = 0.54$ and 0.53 m/s²). Figure 27a shows the spectrum Fourier analyses for the lateral seismic responses of the superstructure mass of the heavy bridge of $M_{st} = 700$ t for bridges with the three studied configurations (parallel, perpendicular, and crossing). The maximum dominant frequency ($F = 0.7$ Hz) was obtained for the parallel bridge configuration, while the dominant frequencies of the crossing and perpendicular bridges' configurations were 0.473 and 0.4 Hz, respectively, with much smaller amplitudes. Conversely, for the light bridge of $M_{st} = 350$ t, the maximum dominant frequency ($F = 0.709$ Hz) was attained for the crossing bridge configuration with a slight amplitude, while the dominant frequency of the perpendicular bridges is $F = 0.7$ Hz and the dominant frequency of the parallel bridges is $F = 0.6$ Hz with much bigger amplitude as illustrated in Figure 27b.

3.2 Two bridges with superstructure mass ratio (300%)

3.2.1 Effect of inter-bridge spacing

A set of numerical analyses have been carried out to examine the influence of inter-bridge spacing on the (SSSI) effect between three different parallel bridges with superstructure masses ratio of 300%. The same geometrical and mechanical characteristics mentioned in section 2.1 for the light bridge of $M_{st} = 350$ t as shown in Figure 2a and for the heavy bridge of $M_{st} = 1050$ t as shown in Figure 2c have been adopted. The numerical study has been performed under the velocity record of the Turkey earthquake (Kocaeli, 1999) and for a range of inter-bridge spacing of precisely $S = 20, 30,$ and 40 m. Figure 28 reveals the 3D meshed model used in the analyses.

3.2.1.1 Results and discussion

Predictably, the soil plasticity under the isolated heavy bridge of $M_{st} = 1050$ t has been prolonged deeper than the one under the isolated light bridge of $M_{st} = 350$ t, except under the cap limits of the light bridge in the x-direction, where the plasticity extended to about two-thirds of the soil depth as shown in Figure 29. However, the (SSSI) effect resulting from the interaction between the three dissimilar bridges has considerably changed the plasticity extension under the three bridges as illustrated in Figure 30. The plasticity prolongation in the zones under the light bridges of $M_{st} = 350$ t is much deeper than the one under the central heavy bridge of $M_{st} = 1050$ t. Furthermore,

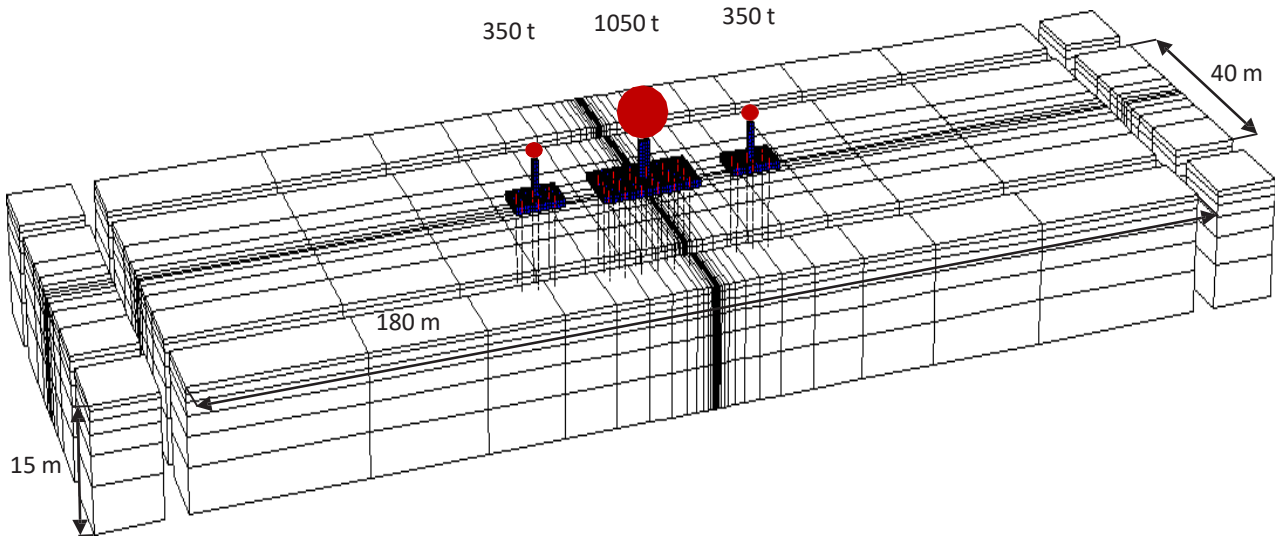


Figure 28: Parallel bridges system 3D numerical mesh with adsorbing boundaries (552 structural elements and 33,072 nodes).

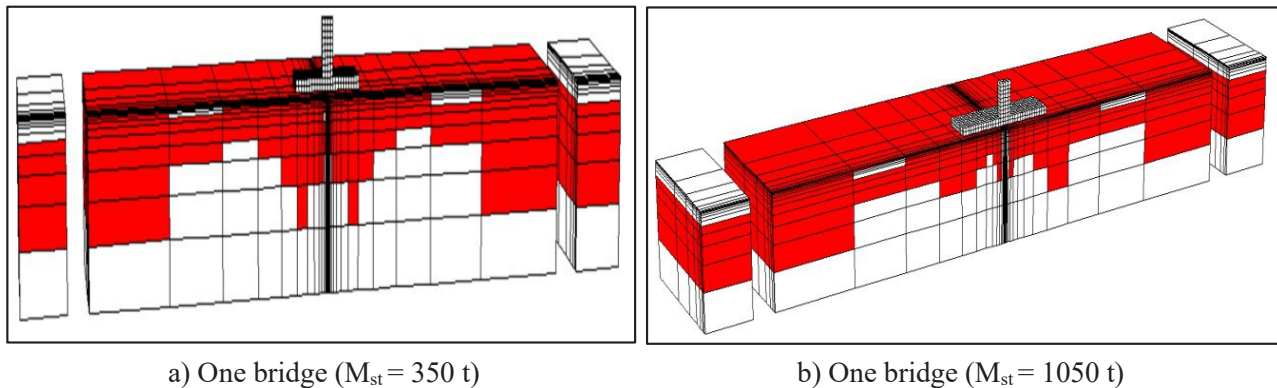


Figure 29: Distribution of plasticity for two single isolated bridges.

Figure 30 reflects the negligible impact of the inter-bridge spacing on plasticizing of the soil. Furthermore, Figure 30 reflects the negligible impact of the inter-bridge spacing on plasticizing of the soil. Table 9 reveals the valuable effect of (SSSI) on both acceleration of the superstructure and the internal forces induced in the piles. In further detail, the mass accelerations of the heavy bridge of $M_{st} = 1050 \text{ t}$ and the light bridge of $M_{st} = 350 \text{ t}$ dropped sharply by 71.8% and 42.28%, respectively. Similarly, the bending moment induced in the piles of the heavy bridge ($M_{st} = 1050 \text{ t}$) and light bridge ($M_{st} = 350 \text{ t}$) decreased considerably by 42.6% and 52.8%, respectively. In a similar manner, the shear force induced in the piles of the heavy bridge significantly reduced by 77.7% and by a much inferior ratio for piles of the light bridge (7%). A slight effect of the inter-bridge spacing is highlighted in Table 9 and Figures 31a–34a. More precisely, the bending moment provoked

in the piles of the heavy and light bridges increased by 10.47% and 7.17%, respectively, with the inter-bridge spacing increase. Similarly, the shear force induced in the piles of the heavy and light bridges increased by 7.2% and 14.38%, respectively, with augmentation of the inter-bridge spacing, as shown in Figures 31b–34b. It must be mentioned that all the maximum internal forces induced in the piles have been reported in the top of the piles, except the maximum shear force in the piles of the light bridge, which was obtained in the central part of the piles.

Similarly, the shear force induced in the corner piles of the bridge ($M_{st} = 350 \text{ t}$) decreased by 4.96% with an increase of inter-bridge spacing as described in Figure 33b. In contrast, the bending moment in the corner piles and the internal forces (bending moment and shear force) in the central piles of the bridge of $M_{st} = 350 \text{ t}$ varied marginally (up to 11%) without showing an evident trend

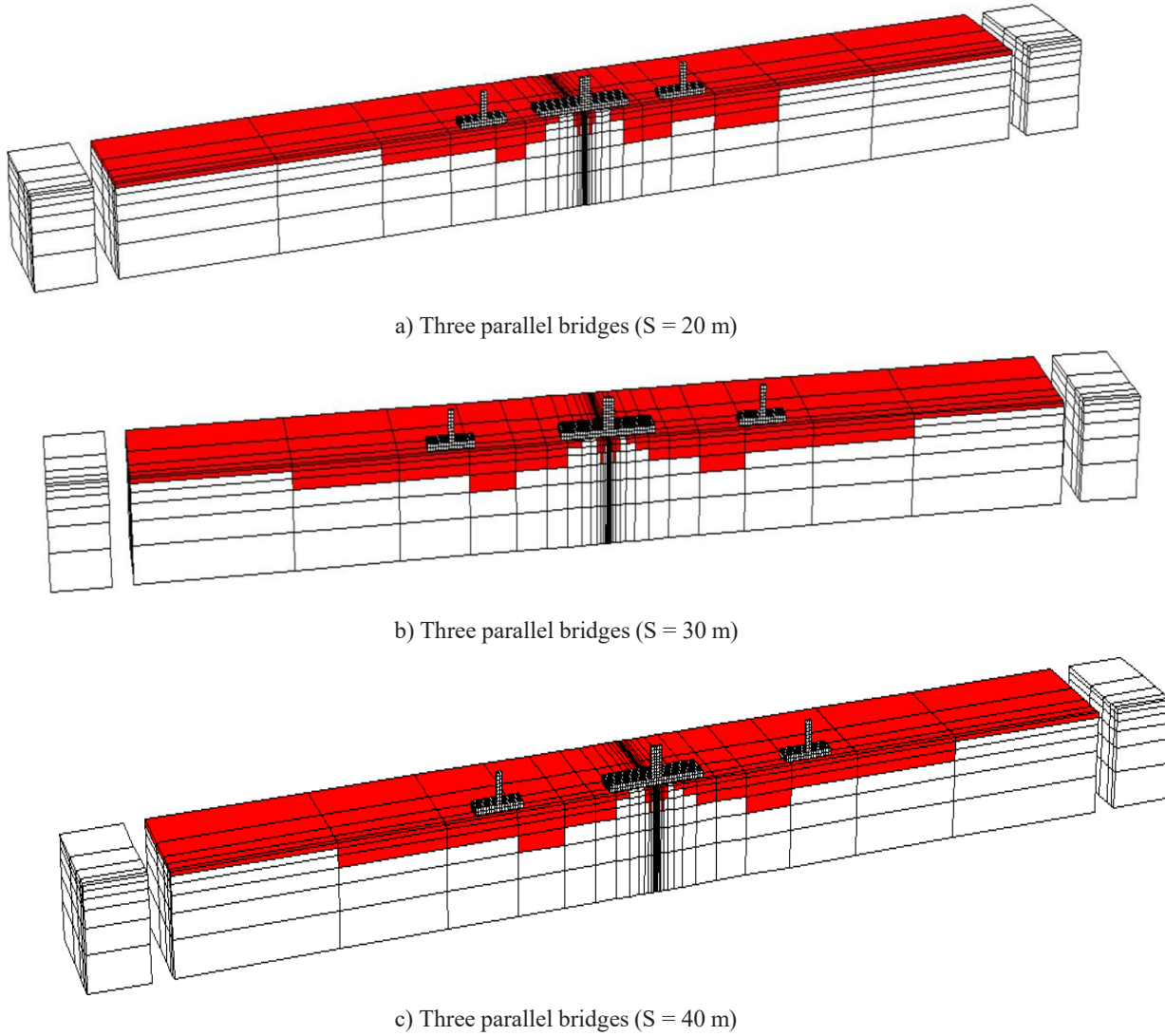


Figure 30: Distribution of plasticity (red zones) for different spacing between the three dissimilar bridges ($M_{st} = 350, 1050$ T, and 350 t).

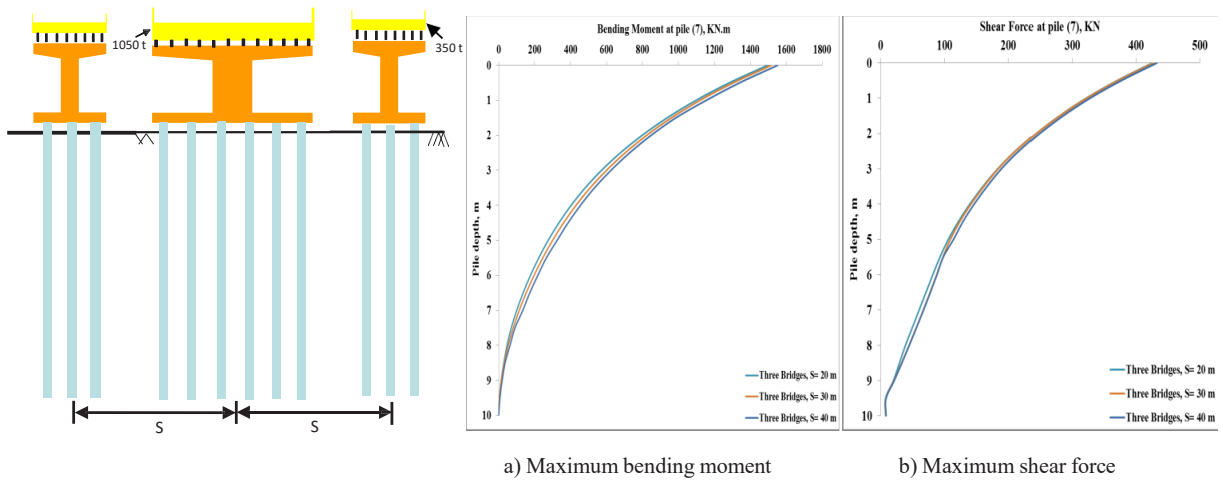
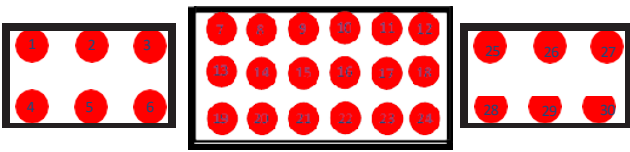


Figure 31: Three dissimilar parallel bridges: Internal forces at corner pile (7) of the bridge (1050 t).

Table 9: Influence of inter-bridge spacing on the seismic response of three dissimilar parallel bridges system



S (m)	ast (m/s ²)	acap (m/s ²)	Internal forces									
			Central piles				Corner piles					
			Pile (2) (Mst = 350 t)		Pile (15) (Mst = 1050 t)		Pile (1) (Mst = 350 t)		Pile (7) (Mst = 1050 t)			
			Mmax (kN m)	Tmax (kN)	Mmax (kN m)	Tmax (kN)	Mmax (kN m)	Tmax (kN)	Mmax (kN m)	Tmax (kN)		
One bridge (Mst = 350 t and S = 0)	20.1	11.5	3979	1268			4093	1330				
One bridge (Mst = 1050 t and S = 0)	20.53	12.49			2196	1325			2061	1294		
S (m)	Bridge (Mst = 350 t)		Bridge (Mst = 1050 t)		Three dissimilar bridges							
	Ast	acap	Ast	acap	Pile (2) (Mst = 350 t)	Pile (15) (Mst = 1050 t)	Pile (1) (Mst = 350 t)	Pile (7) (Mst = 1050 t)				
20 m	11.6	11.6	5.78	4.58	2091	1189	1260	294.8	1929	1236	1496	426.3
30 m	12.1	12.2	5.95	4.79	2166	1271	1322	305.4	1969	1283	1517	428
40 m	12.7	12.7	6.15	5.12	2241	1360	1392	316	2017	1333	1552	433

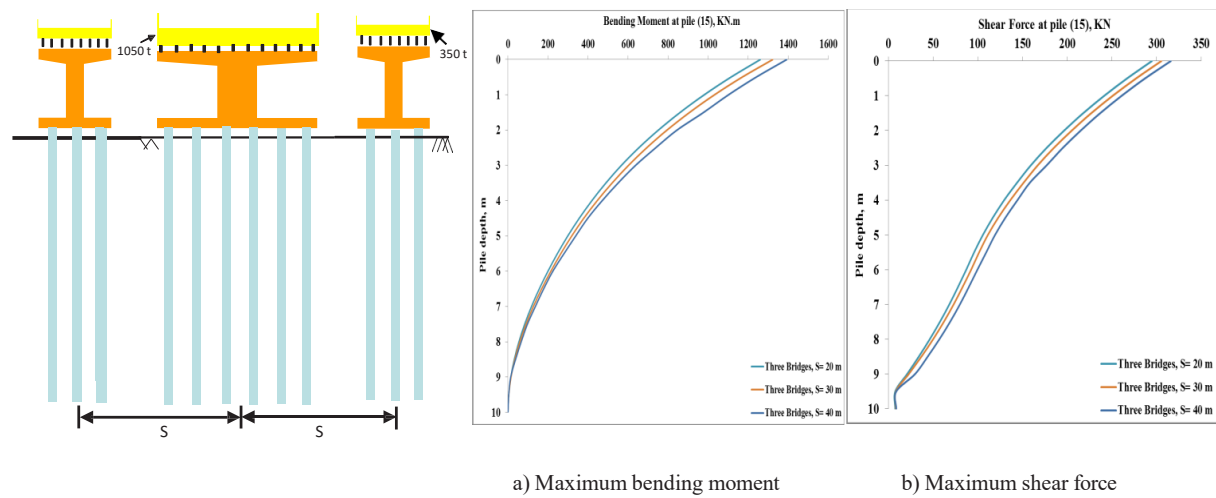


Figure 32: Three dissimilar parallel bridges: Internal forces at corner pile (15) of the bridge (1050 t).

as shown in Table 9 and Figures 33 and 34. It is worth noting that the maximum bending induced in the piles of the bridge of $M_{st} = 350$ t was in the central part of the piles according to Figures 33a and 34a, while all the other internal forces were obtained in the heads of the pile as shown in Figures 33b and 34b.

Spectral velocity analyses of Fourier presented in Figure 36 exhibit a negligible effect of inter-bridge spacing on the dominant frequencies for the studied spacing of $S = 20, 30,$ and 40 m between the three bridges. The dominant frequency was almost constant ($F = 0.827$ Hz for the heavy bridge of $M_{st} = 1050$ t and $F = 0.709$ Hz for the light bridge of $M_{st} = 350$ t).

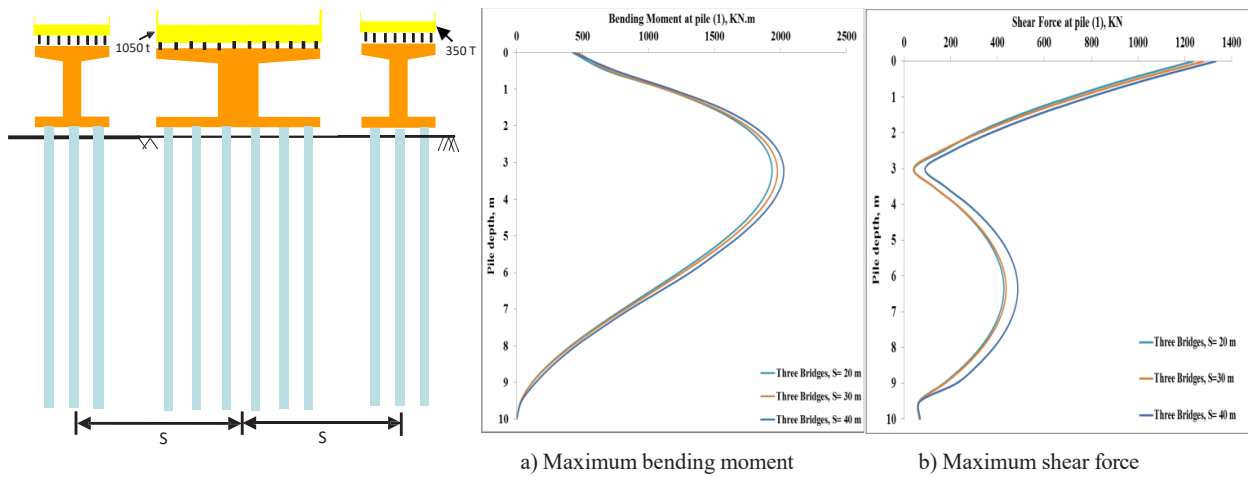


Figure 33: Three dissimilar parallel bridges: Internal forces at corner pile (1) of the bridge (350 t).

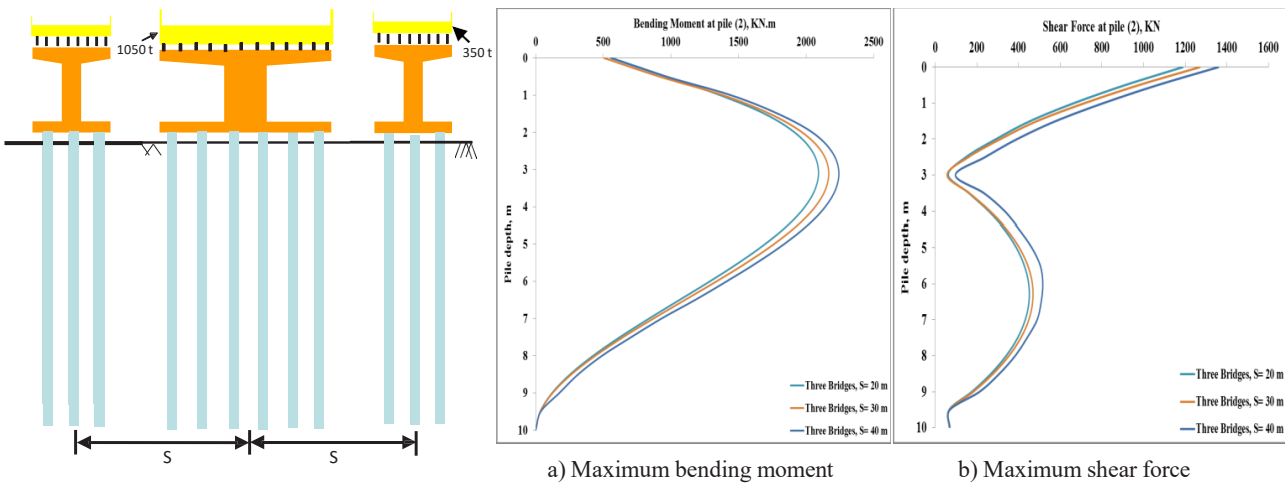


Figure 34: Three dissimilar parallel bridges: Internal forces at central pile (2) of the bridge (350 t).

3.2.2 Effect of bridge plan alignment with respect to each other and the seismic loading direction

Two additional numerical analyses were carried out to examine the effect of the perpendicular and crossing bridges configurations on the overall effect of SSSI. The analyses were performed for the same geometrical and mechanical properties used in the former section (3.2.1) while choosing the inter-bridge spacing of $S = 20$ m as shown in Figures 37 and 38. The numerical analyses were conducted under the seismic loading record of Turkey (Kocaeli, 1999). The employed mesh shown in Figures 37 and 38 includes 8104 zones of eight nodes and 690 3D structural elements of two nodes. Unpredictably, the plasticity under the isolated light perpendicular bridge of $M_{st} = 350$ t prolonged heavily and deeply to the base of the soil, whereas the plasticity spread was substantially

smaller under the central portion of the cap of the heavy perpendicular bridge of $M_{st} = 1050$ t, as illustrated in Figure 39. The interaction between the three bridges incited a substantial change in plasticity extension through the soil. The interaction between the three bridges shown in Figure 40a reduced the plasticity under the heavy bridge of $M_{st} = 1050$ t considerably, with a slight effect on the zones under the light bridge of $M_{st} = 350$ t and inter-bridge zones. Moreover, Figure 40b shows that the plasticity extension almost vanished under the three bridges in the case of interaction between three perpendicular bridges, but it increased considerably under the heavy bridge for the crossing configuration as shown in Figure 40c. Table 10 elucidates the valuable impact of (SSSI) on both superstructure acceleration and the internal forces induced in the piles. Due to the interaction between the three bridges, the mass and cap accelerations of the heavy

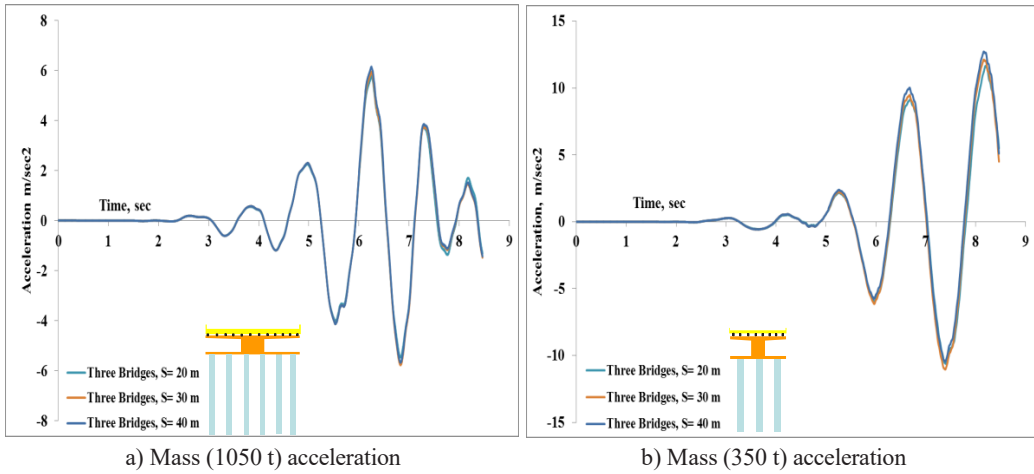


Figure 35: Three dissimilar parallel bridges: Masses accelerations.

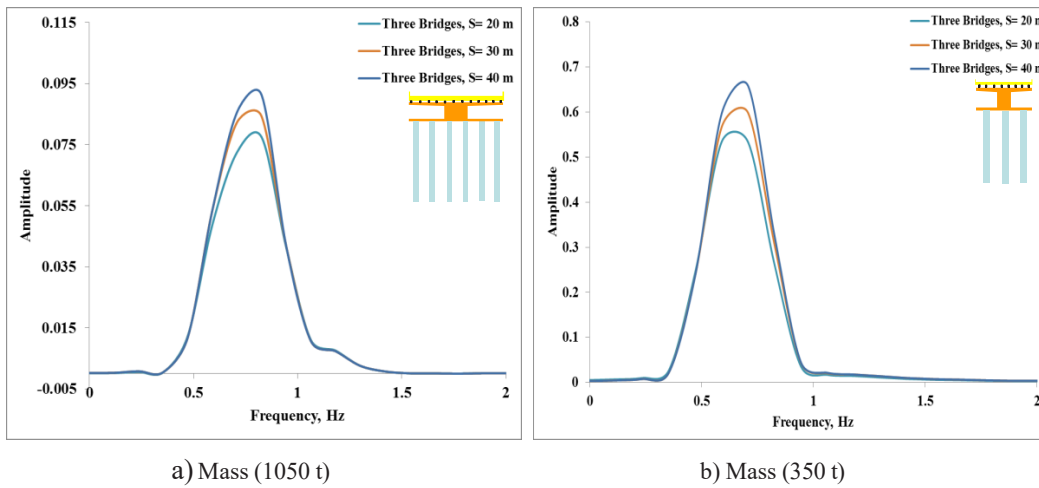


Figure 36: Three dissimilar parallel bridges: Fourier spectra diagram.

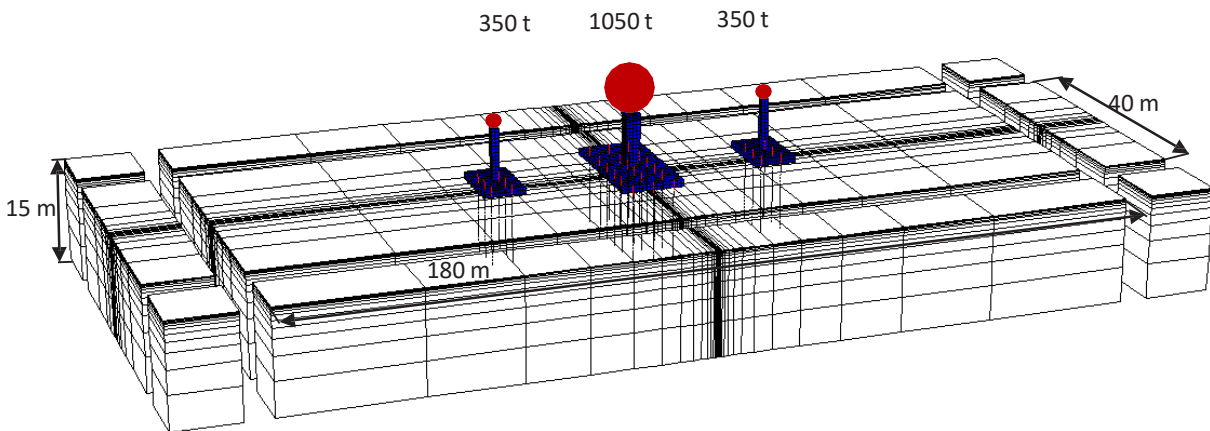


Figure 37: Bridge–soil–bridge system 3D numerical mesh with adsorbing boundaries (690 structural elements and 78,286 nodes).

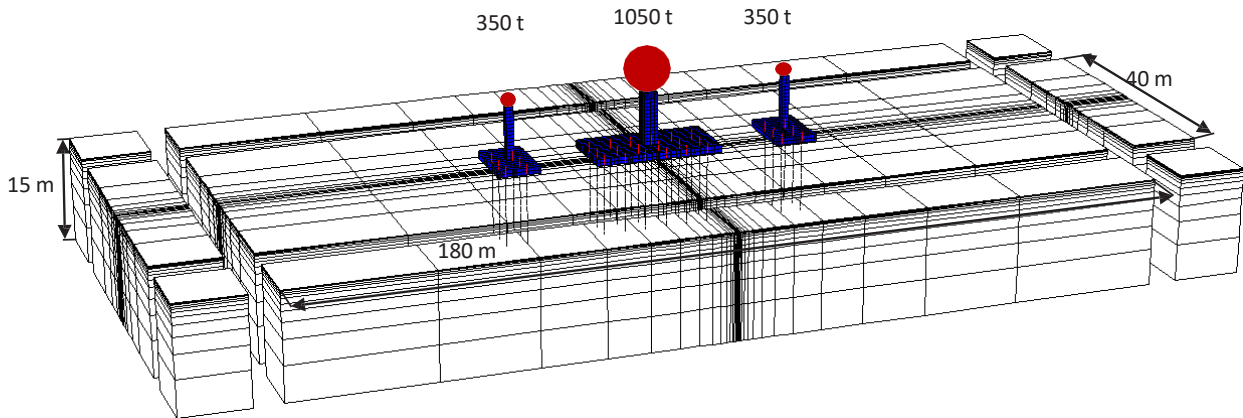


Figure 38: Bridge–soil–bridge system 3D numerical mesh with adsorbing boundaries (690 structural elements and 78,286 nodes).

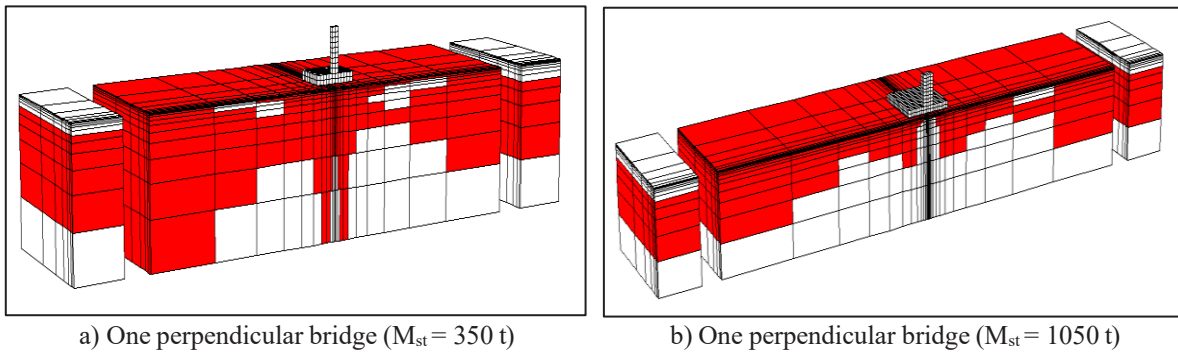


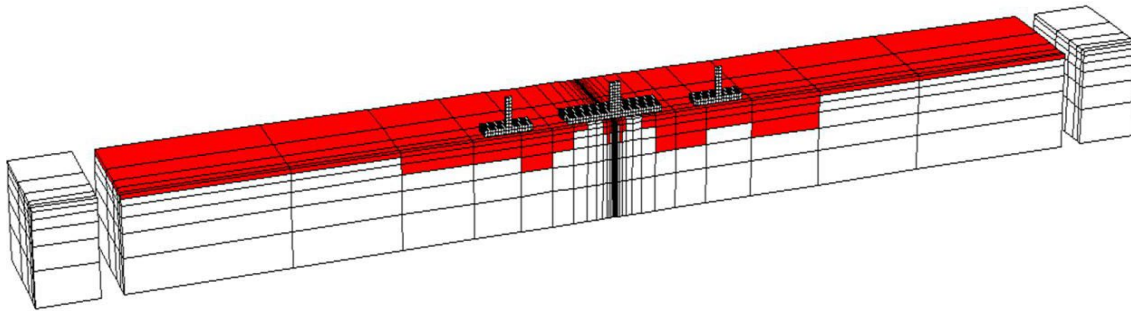
Figure 39: Distribution of plasticity for two single isolated bridges ($M_{st} = 350$ and 1050 t).

bridge hugely reduced by 86.3% and 90.63%, respectively. Similarly, the mass and cap accelerations of the light bridge considerably dropped by 97.46% and 45.2%, respectively. Moreover, the (SSSI) effects incited a substantial decline in the bending moment and shear force in the piles of the heavy bridge by up to 52.55% and 78.6%, respectively. Similarly, for the piles of the light bridge, the bending moment and the shear force hugely decreased due to the (SSSI) effects by up to 91.18% and 91.27%, respectively.

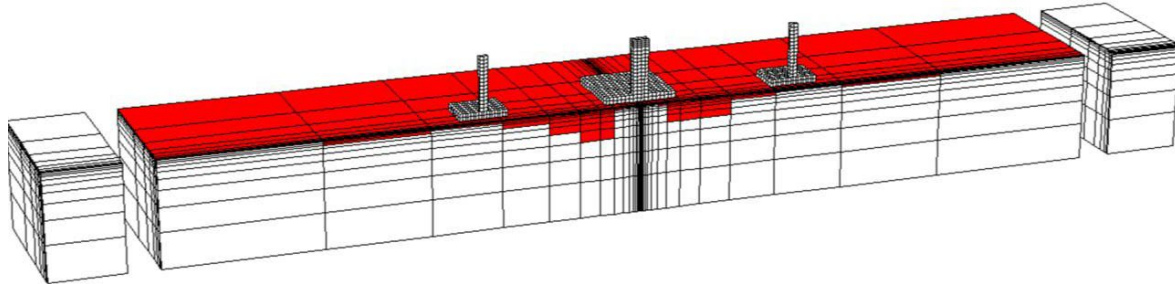
The minimum internal forces (bending moment and shear force) induced in the corner pile (7) of the heavy bridge of $M_{st} = 1050$ T have been obtained for the parallel bridge configurations with a bending moment of $M_{min} = 1496$ kN m and a shear force of $T_{min} = 426.3$ kN as shown in Table 10 and Figure 41. Whereas the maximum bending moment ($M_{max} = 2412$ kN m) and the maximum shear force ($T_{max} = 1274$ kN) have been obtained in the case of crossing bridge configuration. Alongside, the minimum accelerations of the superstructure (mass and cap) accompanied by minimum shear force in the central pile (15) of the heavy bridge ($M_{st} = 1050$ t) occurred in the

case of perpendicular bridges configuration as shown in Table 10 and Figure 42. It should be mentioned that the bending moment and the shear force of the heavy bridge vary by 37.9% and 66.5%, respectively, with the bridge configuration changing between parallel, perpendicular, and crossing configurations, while the configuration change of the bridges has a bigger influence on the superstructure acceleration by variation of up to 74.45% as shown in Table 10.

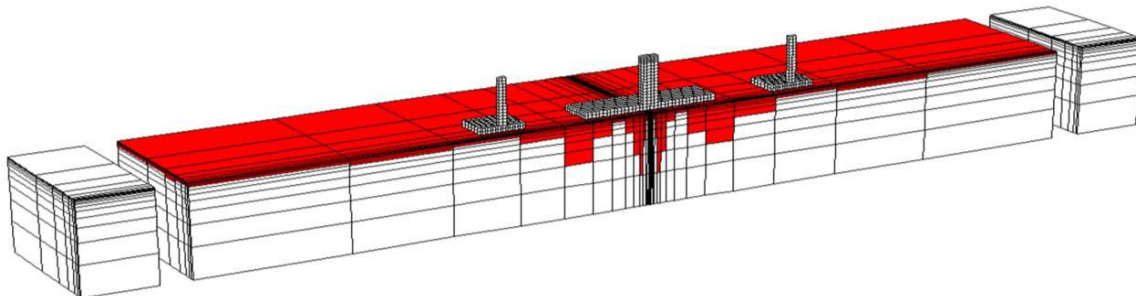
On the contrary, the minimum internal forces (bending moment and shear force) induced in the central and corner piles of the light bridge of $M_{st} = 350$ t were achieved for the configuration of crossing bridges as shown in Table 10 and Figures 43 and 44. Precisely, the minimum bending moment ($M_{min} = 360.8$ kN m) was obtained in the corner pile (1), while the minimum shear force ($T_{min} = 110.6$ kN) was obtained in the central pile (2). Moreover, the minimum superstructure accelerations were also gained for the crossing configuration with mass and cap accelerations of $A_{st} = 0.51$ m/s² and $A_{cap} = 6.3$ m/s², respectively. It is worth noting that the mass



a) Parallel bridges

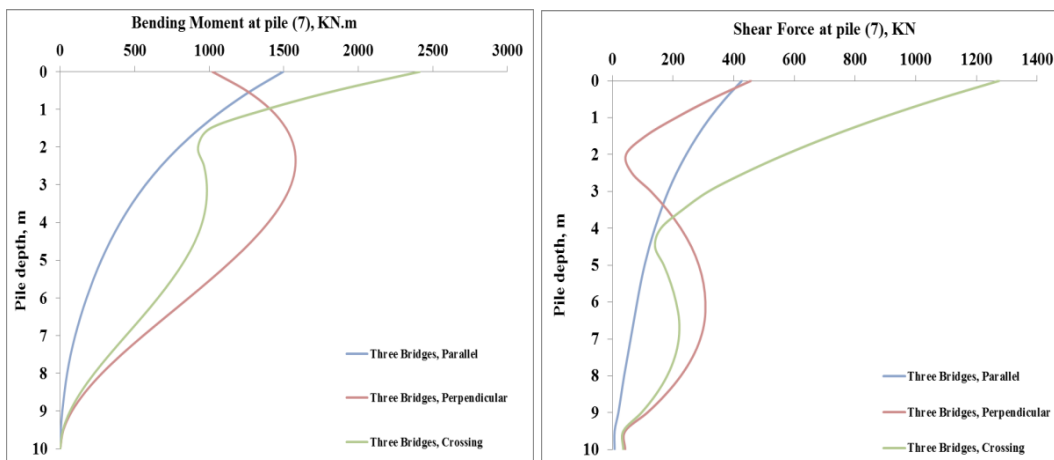


a) Perpendicular bridges



a) Crossing bridges

Figure 40: Distribution of plasticity (red zones) for different positioning of the three dissimilar bridges ($M_{st} = 350, 1050, \text{ and } 350 \text{ t}$).



a) Maximum bending moment

b) Maximum shear force

Figure 41: Three dissimilar bridges: Internal forces at corner pile (7) of the bridge (1050 t).

Table 10: Influence of different positioning of three dissimilar bridges on the seismic response system.

Position	ast		acap (m/s ²)		Internal forces							
	(m/s ²)				Central piles				Corner piles			
					Pile (2) (Mst = 350 t)		Pile (15) (Mst = 1050 t)		Pile (1) (Mst = 350 t)		Pile (7) (Mst = 1050 t)	
	Mmax (kN m)	Tmax (kN)	Mmax (kN m)	Tmax (kN)	Mmax (kN m)	Tmax (kN)	Mmax (kN m)	Tmax (kN)	Mmax (kN m)	Tmax (kN)		
One perpendicular bridge (Mst = 350 t)	20.1		11.5		3979	1268			4093	1330		
One perpendicular bridge (Mst = 1050 t)	20.53		12.49				2196	1325			2061	1294
Position	Bridge (Mst = 350 t)		Bridge (Mst = 1050 t)		Three dissimilar bridges							
	ast	acap	ast	acap	Pile (2) (Mst = 350 t)		Pile (15) (Mst = 1050 t)		Pile (1) (Mst = 350 t)		Pile (7) (Mst = 1050 t)	
Parallel	11.6	11.6	5.78	4.58	2091	1189	1260	294.8	1929	1236	1496	426.3
Perpendicular	0.54	6.47	2.81	1.17	411.8	113.4	1580	282.7	388	130.5	1578	456.2
Crossing	0.51	6.3	5.67	2.39	370.2	110.6	1042	589.7	360.8	123.2	2412	1274

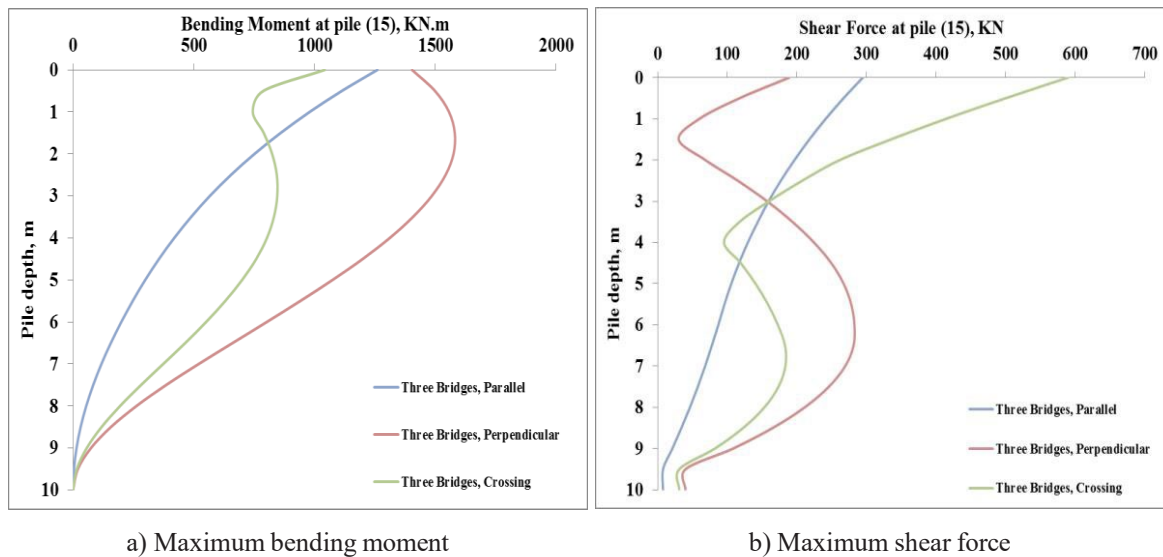


Figure 42: Three dissimilar bridges: Internal forces at central pile (15) of the bridge (1050 t).

accelerations of the light bridges for the perpendicular and crossing configurations were hugely smaller than the cap accelerations. Table 10 indicates an evident tendency to a significant drop in the superstructure acceleration, bending moment, and shear force by up to 95.6%, 82.3%, and 90.69%, respectively, with the bridge configuration change starting from parallel to perpendicular and finally crossing bridges.

Table 10 and Figure 45a reveal a significant drop in the acceleration of the lumped mass of the heavy bridge of $M_{st} = 1050$ t with $A_{st} = 2.81$ m/s² in the case of perpendicular bridges configuration, while the mass acceleration values for the parallel and crossing bridges configurations are very close. In addition, the time lag between the three accelerations is worth noting. On the contrary, the maximum lumped mass acceleration of the light bridge of

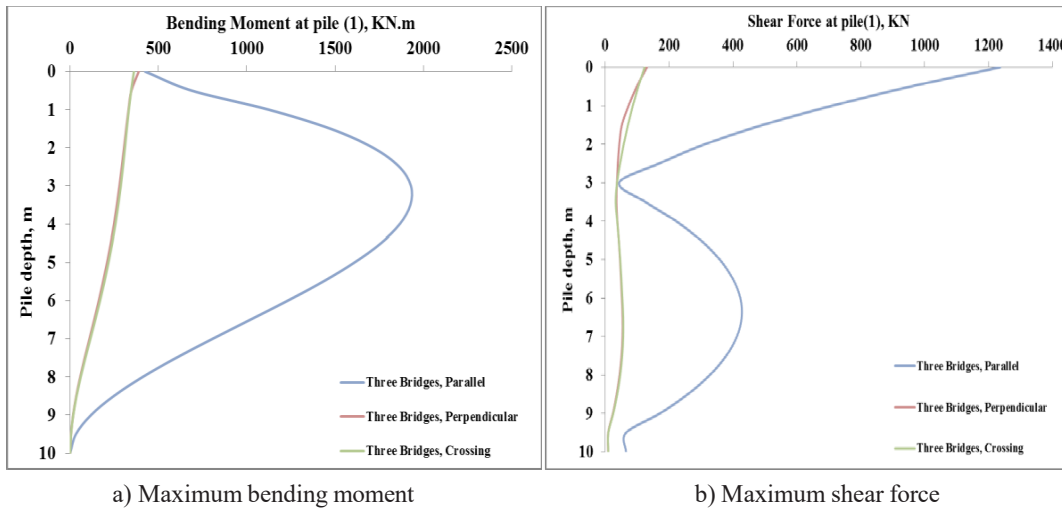


Figure 43: Three dissimilar bridges: Internal forces at corner pile (1) of the bridge (350 t).

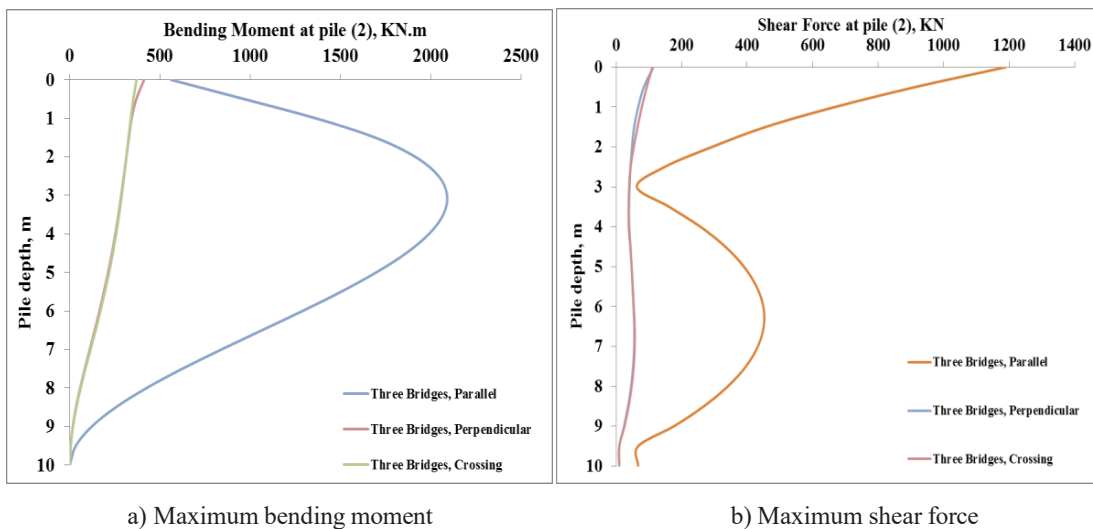


Figure 44: Three dissimilar bridges: Internal forces at central pile (2) of the bridge (350 t).

$M_{st} = 350$ t was obtained for the configuration of parallel bridges with $A_{st} = 11.6$ m/s², whereas the mass accelerations for the perpendicular and crossing configurations were hugely smaller and had a semi-constant value as shown in Figure 45b. Figure 46a shows the Fourier spectral analyses of the lumped mass velocity of $M_{st} = 1050$ t for the three studied configurations. The dominant frequency of the parallel configuration $F = 0.827$ Hz dropped to $F = 0.6$ Hz for the crossing configuration and to $F = 0.473$ Hz for the perpendicular configuration. Conversely, for the dominant frequency of the lumped mass of $M_{st} = 350$ T shown in Figure 46b, the dominant frequencies were constant ($F = 0.7$ Hz) for the three configurations, but with much smaller amplitude for the perpendicular and crossing configurations.

4 Conclusions

An extensive set of detailed 3D numerical analyses have been performed to evaluate the effects of SSSI between three dissimilar neighboring bridges under seismic excitations. The analyses have focused on the impact of the adjacent superstructures' lumped mass ratios (200% and 300%) on the (SSSI) effect. Moreover, the effects of prominent factors such as the inter-bridge spacing and the position of the three neighboring bridges toward each other and toward the seismic loading direction have been investigated. The 3D code (FLAC 3D) based on the finite difference elements method has been used in the numerical calculations, in which hysteretic damping has been considered for both soil and bridges, and linear

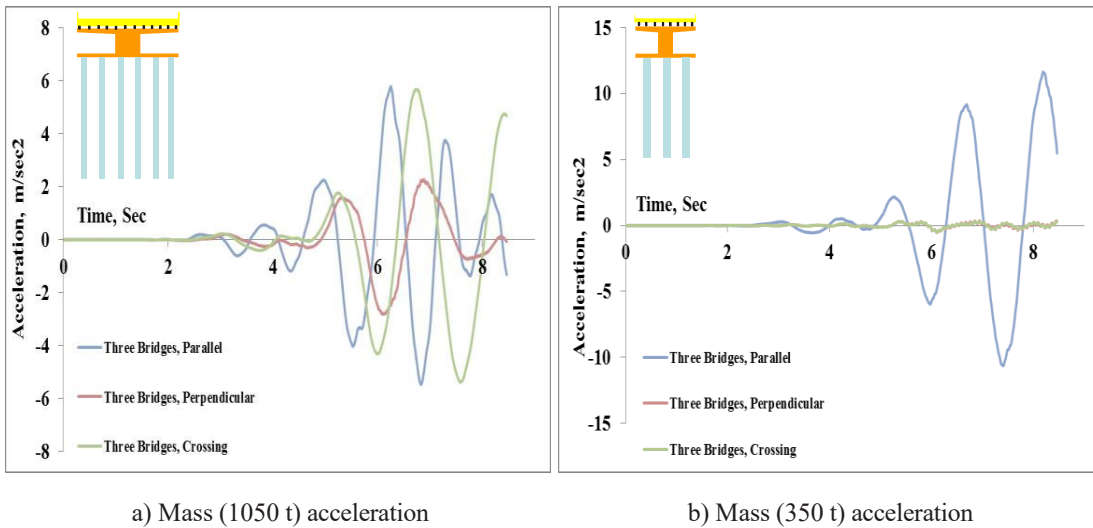


Figure 45: Three dissimilar bridges: Masses accelerations.

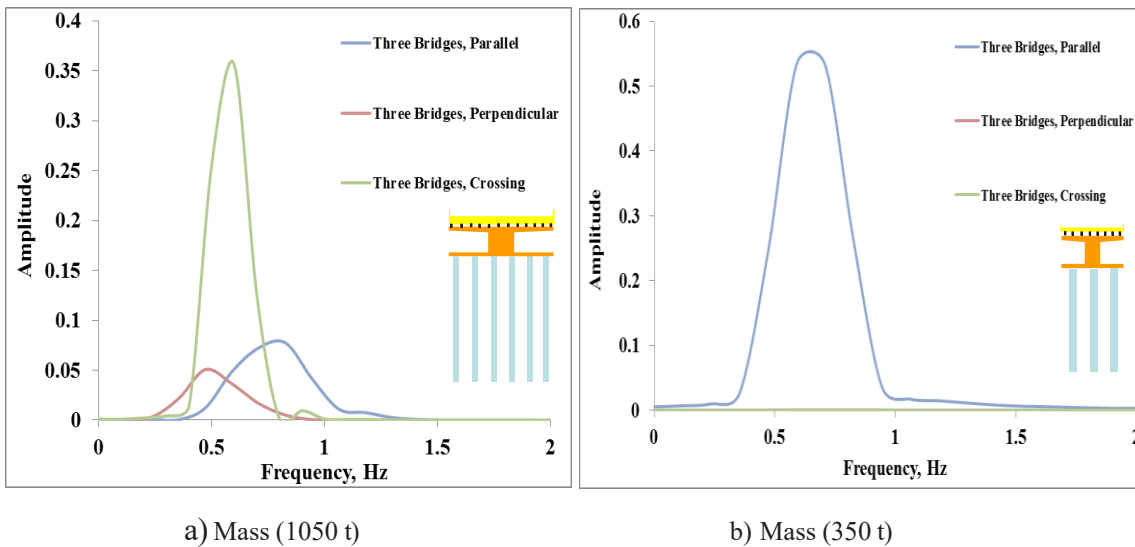


Figure 46: Three dissimilar bridges: Fourier spectra diagram.

assumptions have been put forward for the bridges and nonlinear assumptions for the soil behavior to simulate the realistic seismic behavior of the soil in this rigorous 3D modeling. These numerical analyses have been performed under a real single record of Turkey (Kocaeli, 1999). Further analysis under different earthquake records will be pursued in the future to confirm the conclusions drawn.

The main question of this research is in what situations the seismic SSSI effect could be beneficial or detrimental for the individual elements of the system.

Furthermore, what are the key factors that may control the degree of multi-structural interactions? This research

has led to the following principal conclusions based on the cases studied:

- Intriguingly, the results revealed substantial beneficial effects of (SSSI) between the three dissimilar bridges on both superstructure acceleration and the internal forces induced in the piles, particularly for the case of neighboring superstructures’ lumped mass ratio of 300%. Differently, the (SSSI) effects between two identical bridges ($M_{st} = 350\text{ t}$) had modest effect (rather positive) on the seismic response of the two bridges and the internal forces induced in the piles, according to the results of Alfach and Al Helwani (2019).

- The consideration of (SSSI) effect between dissimilar bridges incites a sharp drop in the superstructure acceleration (up to 90.63%) for the case of adjacent superstructures' mass ratio of 300%.
- The (SSSI) effect sharply reduces the bending moment and the shear force induced in the piles by up to 91.18% and 91.27%, respectively, for the case of neighboring superstructures' lumped mass ratio of 300%.
- Substantially, in case of interaction between adjacent different bridges, the level of (SSSI) effect on the response of the bridges highly depend on the neighboring superstructures' lumped mass ratios.
- The inter-bridge spacings had slight effect on superstructure acceleration by reduction of the closest spacing (up to 6.9%). Similarly, the bending moment and the shear force declined by up to 10.47% and 14.38%, respectively, which agrees with the conclusions obtained by Alfach and Al Helwani (2019) for the effect of inter-bridge spacing between two identical bridges of ($M_{st} = 350$ t).
- Finally, the geometrical position of the bridges toward each other and toward the seismic loading direction has significant impact on the seismic behavior of the system, particularly for the light bridges, which is reflected by huge reduction for the crossing case of the superstructure acceleration, bending moment, and the shear force by ratios up to 97.46%, 91.18%, and 91.27%, respectively, which agrees with the results of Alfach and Al Helwani (2019) for the interaction between two identical bridges of $M_{st} = 350$ t.

References

- [1] Kim, Kyung Tae., 2014. Three-dimensional nonlinear seismic response of large-scale ground-structure systems. *University of California*, San Diego. Ph.D. dissertation, La Jolla, CA. <https://escholarship.org/uc/item/3x7237xp>
- [2] Bolisetti, C., and Whittaker, A.S., 2015. Site Response, Soil-Structure Interaction and Structure-Soil- Structure Interaction for Performance Assessment of Buildings and Nuclear Structures, *Technical Report MCEER-15-0002*, MCEER, University at Buffalo. <http://www.buffalo.edu/mceer/catalog.host.html/content/shared/www/mceer/publications/MCEER-15-0002.detail.html>
- [3] Lu, Yang., Li, Bo., Xiong, Feng., Ge, Qi., Zhao, Peng., Liu, Yang., 2020. Simple discrete models for dynamic structure-soil-structure interaction analysis. *Engineering Structures*. Volume 206, 110188. <https://doi.org/10.1016/j.engstruct.2020.110188>
- [4] Bybordiani, M., and Arici, Y., 2019. Structure-soil-structure interaction of adjacent buildings subjected to seismic loading. *Earthq. Eng. Struct. Dyn*, 48, 731–748. <https://doi.org/10.1002/eqe.3162>
- [5] Isbiloglu, Y., Taborda, R., Bielak, J., 2015. Coupled soil-structure interaction effects of building clusters during earthquakes. *Earthquake Spectra*, Vol.31, Issue1. <https://doi.org/10.1193/102412EQS315M>
- [6] Bolisetti, C., and Whittaker, A.S., 2020. Numerical investigations of structure-soil-structure interaction in buildings, *Engineering Structures*, 215 – 110709. <https://doi.org/10.1016/j.engstruct.2020.110709>
- [7] Ogut, oguz can., 2017. Soil-Structure Interaction Effect of Embedded Foundation and Adjacent Buildings on Response Characteristics of Superstructures. *Nagoya University*, Nagoya. Ph.D. dissertation, Japan.
- [8] Yahyai, M., Mirtaheri, M., Mahoutian, M., Daryan, A. S. & Assareh, M. A., 2008. Soil structure interaction between two adjacent buildings under earthquake load. *American Journal of Engineering and Applied Sciences*, 1(2), 121-125. <https://doi.org/10.3844/ajeassp.2008.121.125>
- [9] Álamo, Meneses., G. M., Padrón Hernández, L. A., Aznárez González, J. J., & Maeso Fortuny, O., 2015. Structure-soil-structure interaction effects on the dynamic response of piled structures under obliquely-incident seismic shear waves. *Soil dynamics and earthquake engineering*, Vol.78, 142-153. <https://doi.org/10.1016/j.soildyn.2015.07.013>
- [10] Rahgozar, M.A., 2015. Accounting for soil nonlinearity in three-dimensional seismic structure-soil- structure-interaction analyses of adjacent tall buildings structures. *International journal of civil engineering*, 13 (3 and 4B) ,213-225. DOI: 10.22068/IJCE.13.3.213
- [11] Nakamura, S., Nakamura, N., Suzuki, T., Inoda, K., Kosaka, K., 2012. Study on the Influence of Irregular Ground and Adjacent Building on the Seismic Response of Nuclear Power Plant Building. *15 WCEE*, LISBOA 2012. https://www.iitk.ac.in/nicee/wcee/article/WCEE2012_1367.pdf
- [12] Roy, Christine., Bolourchi, Said., & Eggers, Daniel., 2015. Significance of structure-soil-structure interaction for closely spaced structures. *Nuclear Engineering and Design*, Vol. 295, 680-687. <https://doi.org/10.1016/j.nucengdes.2015.07.067>
- [13] Barrios, G., Chouw, N., 2015. Experimental investigations of interaction between structure, soil and adjacent structures, *In NZSEE Conference*, New Zealand.
- [14] Ikeda, Y., Shimomura, Y., Nakamura, M., Haneda, O., Arai, T., 2004. Dynamic influence of adjacent structures on pile foundation based on forced vibration tests and earthquake observation. *13th World Conference on Earthquake Engineering*, Vancouver, B.C., Canada. https://www.iitk.ac.in/nicee/wcee/article/13_1869.pdf
- [15] Larkin, T., Qin, X., Chouw, N., 2016. Effect of local site on sfsi of clustered structures. *Conference: NatHaz 16 - Soil characterization and site effects*, S. Miguel, Portugal
- [16] Ge, Qi., Xiong, Feng., Zhang, Jing., 2020. Study on dynamic structure-soil-structure interaction of three adjacent tall buildings subjected to seismic loading. *Sustainability*, 12(1), 336. <https://doi.org/10.3390/su12010336>
- [17] Trombetta, N.W., Mason, H.B., Hutchinson Tara, C., Zupan Joshua, D., Bray Jonathan, D., Kutter Bruce, L., 2014. Nonlinear soil-foundation-structure and structure-soil-structure interaction: centrifuge test observations. *Journal of Geotechnical and Geoenvironmental Engineering*, Vol. 140, Issue 5. [https://doi.org/10.1061/\(ASCE\)GT.1943-5606.0001074](https://doi.org/10.1061/(ASCE)GT.1943-5606.0001074)

- [18] Andersen, L.V., Peplow, A., Bucinkas, P., Persson, P., Persson, K., 2017. Variation in models for simple dynamic structure–soil–structure interaction problems. *Procedia Engineering*, Vol. 199. <https://doi.org/10.1016/j.proeng.2017.09.190>
- [19] Gan, Jinsong., Li, Peizhen and Liu, Qiang., Chen, Jiang., 2017. Shaking table test of dynamic interaction of soil – high-rise buildings. *European Journal of Environmental and Civil Engineering*, 21:3, 249-271, <https://doi.org/10.1080/19648189.2015.1110057>
- [20] Wang, Huai-feng., 2018. Structure-soil-structure interaction between underground structure and surface structure, Earthquakes - Forecast, *Prognosis and Earthquake Resistant Construction*, Valentina Svalova, IntechOpen. DOI: 10.5772/intechopen.76243
- [21] Bard, P. Y., Boutin, C., Dietz, M. S., Schwan, L., 2013. Study of multi-building interactions and site-city effects through an idealized experimental model, *Seismic Engineering Research Infrastructures for European Synergies*, Project No.: 227887, Final report. http://www.series.upatras.gr/sites/default/files/file/SERIES_SCIES_final%20report.pdf
- [22] Schwan, L., Boutin, C., Padrón, L.A., Dietz, M.S., Bard, P.Y., Taylor, C., 2016. Site-city interaction: theoretical, numerical and experimental crossed-analysis. *Geophys. J. Int*, Vol. 205, Issue 2, 1006-1031. <https://doi.org/10.1093/gji/ggw049>
- [23] Mason, H. B., Trombetta, N. W., Gille, S., Lund, J., Zupan, J., Jones, K. C., Puangnak, H., Bolisetti, C., Bray, J., Hutchinson, T., Fiegel, G., Kutter, B. L., Whittaker, A. S., 2010a. Seismic Performance Assessment in Dense Urban Environments: Centrifuge Data Report for HBM02 (Test 1). *Davis Center for Geotechnical Modeling, University of California*. Davis, California.
- [24] Ngo, Van-Linh., Kim, Jae-Min., Chang, Soo-Hyuk and Lee, Changho., 2019. Effect of height ratio and mass ratio on structure-soil-structure interaction of two structures using centrifugal experiment. *Appl. Sci*, 9(3), 526. <https://doi.org/10.3390/app9030526>
- [25] Alam, Md Iftekharul., Kim, Dookie., 2014. Spatially varying Ground Motion Effects on Seismic Response of Adjacent Structures Considering Soil-Structure Interaction. *Advances in Structural Engineering*, Vol. 17 No. 1 2014. <https://doi.org/10.1260/1369-4332.17.1.131>
- [26] Ritter, Stefan., 2017. Experiments in tunnel-soil-structure interaction. *Thesis (PhD)*. Department of Engineering, University of Cambridge.
- [27] Alfach, Mohanad Talal., 2023. “Effect of Structure-Soil-Structure Interaction (SSSI) between three dissimilar adjacent bridges”. *Geotechnical and Geological Engineering*. <https://doi.org/10.1007/s10706-023-02468-8>
- [28] Knappett, J.A., Madden, P., Caucis, K., 2015. Seismic structure-soil-structure interaction between pairs of adjacent building structures. *Geotechnique*, 65, 429–441. <https://doi.org/10.1680/geot.SIP.14.P.059>
- [29] Ada, M., and Ayyaz, Y., 2019. The structure-soil-structure interaction effects on the response of the neighbouring frame structures. *Latin American Journal of Solids and Structures*,16(8), e224. <https://doi.org/10.1590/1679-78255762>
- [30] Vicencio, F., Alexander, N., Erick, I., 2023. A State-of-the-Art review on Structure-Soil-Structure interaction (SSSI) and Site-City interactions (SCI). *Structures*, Vol. 56. <https://doi.org/10.1016/j.istruc.2023.105002>
- [31] Ghasemzadeh, H., Alibeikloo, M., 2011. Pile–soil–pile interaction in pile groups with batter piles under dynamic loads. *Soil Dynamics and Earthquake Engineering*, Vol. 31, Issue. 8. <https://doi.org/10.1016/j.soildyn.2011.04.005>
- [32] Asgarian, B., Shokrgozar, R., Shahcheraghi, D., and Ghasemzadeh, H., 2018. “Effect of soil pile structure interaction on dynamic characteristics of jacket type offshore platforms,” *Coupled systems mechanics*. 테크노프레스, Vol.1, Issue. 4. <https://doi.org/10.12989/csm.2012.1.4.381>
- [33] Ghasemzadeh, H., Tarzaban, M. & Hajitaheriha, M.M., 2018. Numerical Analysis of Pile–Soil–Pile Interaction in Pile Groups with Batter Piles. *Geotech Geol Eng* 36, 2189–2215. <https://doi.org/10.1007/s10706-018-0456-4>
- [34] Alfach, Mohanad Talal., Al Helwani, Amjad., 2019. Seismic interactions between adjacent and crossing bridges on deep foundations in nonlinear soil. *Geomechanics and Geoengineering*. <https://doi.org/10.1080/17486025.2019.1648883>
- [35] Alfach, Mohanad Talal., 2021. Seismic structure-soil-structure interaction between two different adjacent piled bridges founded in nonlinear soil. *Geomechanics and Geoengineering*. <https://doi.org/10.1080/17486025.2021.1928764>
- [36] Chopra, A. K., 2012. Dynamics of structures theory and applications to earthquake engineering , p. 416. Upper Saddle River: Prentice Hall. ACDSsee print job (gacbe.ac.in)